Pergamon

Carbon Vol. 35, No. 7, pp. 893–916, 1997

0008-6223/97 $17.00 + 0.00

PII: S0008-6223(97)00039-0

ELECTROCHEMICAL BEHAVIOR OF POROUS CARBONS

CHRISTINE A. FRYSZ,[a] XIAOPING SHUI[b] and D. D. L. CHUNG,[b,*]
[a]Wilson Greatbatch Ltd., 10 000 Wehrle Drive, Clarence, NY 14031, U.S.A.
[b]Composite Materials Research Laboratory, Furnas Hall State University of New York at Buffalo, Buffalo, NY 14260-4400, U.S.A.

(*Received* 24 *July* 1996; *accepted in revised form* 4 *February* 1997)

Abstract—The electrochemical behavior of porous carbons based on carbon fibers and those based on phenolic was evaluated by cyclic voltammetry via the Fe^{2+}/Fe^{3+} redox couple. An irreversible electrochemical response obtained from the fiber-based porous carbons was made reversible by coating of the porous carbons with graphite flakes or carbon black; the electron-transfer rate constant k_s and the capacitance were increased, while the electrochemical area was decreased. Porous carbons based on phenolic exhibited variation from batch to batch in their electrochemical behavior, due to contamination by long-chain aliphatic hydrocarbons (comprising $\leq 10\%$ of the porous carbon weight). Their electrochemical performance was rendered consistent from batch to batch and also enhanced (with increased k_s) by cleansing in methylene chloride. The electrochemical areas obtained for phenolic-based porous carbons were larger than those of the fiber-based porous carbons, even though their specific geometric surface areas (per unit volume) were much lower. The electrochemical area decreased with increasing specific geometric surface area (per unit volume) for phenolic-based porous carbons, while the specific electrochemical surface area did not vary much; at a pore density of 30 ppi, the electrochemical area was even higher than that of carbon black, due to the large pore size and the consequent penetrability by the electrolyte. Among the fiber-based porous carbons, both electrochemical area and specific electrochemical area decreased with decreasing specific geometric surface area (increasing fiber length). The 500 ppi phenolic-based porous carbon, after methylene chloride cleansing, exhibited higher k_s than conventional glassy carbon. The fiber-based porous carbons exhibited higher apparent density, lower resistivity and higher compressive strength than those based on phenolic. © 1997 Elsevier Science Ltd

Key Words—A. Carbon fibers, glass-like carbon, D. electrochemical properties, porosity.

1. INTRODUCTION

Porous carbons consist of a continuous matrix of carbon within which is distributed a series of connected open spaces or pores. Primary applications for porous carbons include electrodes, filters, chemical absorbers, molecular sieves, membranes, catalysts and catalyst supports, chemical hardware, mechanical seals, bearings, electrical devices, dental and surgical prosthetic devices and other implants, thermal insulators, lightweight structural elements and structural matrices for composites [1–14]. When used as an electrode, electrochemical processes occur at the carbon surfaces of the open spaces more so than at the outer planar surface, resulting in a three-dimensional electrochemical activity rather than the planar responses characteristic of solid electrodes. As such, the electrochemical behavior of porous carbons is of interest. Because research specific to porous carbon materials is limited, even though porous carbons are a readily available material, and because the electrochemical characterization of porous carbons (i.e. the electron-transfer rate k_s, capacitance C and active electrochemical area A of the porous carbon, all of which define the electrochemical character of materials) has not previously been performed, this work was undertaken. Furthermore, this work systematically studies the effect of carbon fiber length on the mechanical, electrical and electrochemical properties of carbon-fiber-based porous carbons.

The kinetics and reversibility of electrochemical processes strongly depend on the surface of the electrodes. Therefore, surface treatments are commonly applied to electrode materials. These treatments include changes in the surface functional groups, surface crystallographic structure and surface roughness. They may involve chemical treatment, heat treatment, laser treatment, plasma treatment, polishing or other surface activation. In particular, in the case of carbon materials, acid treatment [15–20], heat treatment [21,22], laser treatment [23,24] and electrode polishing procedures [25] have been employed. These treatments tend to increase the oxygen-containing functional groups on the surface of the carbon. In the case of high temperature heat treatment in an inert or reducing atmosphere or in vacuum, graphitization of the carbon can take place, thus changing the crystallographic structure both in the surface and in the bulk. In the case of heat treatment in the presence of oxygen, oxidation of the carbon occurs, thus increasing the amount of oxygen-containing functional groups on the surface and even converting the carbon into CO or CO_2 gases (thereby roughening the surface).

In contrast to the surface modifications mentioned above, this paper involves surface cleansing of the

*Corresponding author.

Table 1. Properties of carbon fibers

Filament diameter	10 μm
Tensile strength	690 MPa
Tensile modulus	48 GPa
Elongation at break	1.4%
Electrical resistivity	$3.0 \times 10^{-3}\ \Omega \cdot$cm
Density	1.6 g cm^{-3}
Carbon content	98% by weight

phenolic-based porous carbons, and particulate additive coating of the fiber-based porous carbons. Cleansing refers to the removal of contaminants from the surface through washing in a solvent. Additive coating refers to the addition of carbon particulates, specifically carbon black (mean diameter of 420 Å, from Chevron, Houston, Texas) and graphite flakes (2 μm wide, 0.5 μm thick, from Asbury Graphite Mills, Inc., Asbury, NJ), to a pitch-based solution, which impregnates the porous carbon and coats as it dries. Neither surface treatment has previously been applied to porous carbons for any purpose, let alone for characterization of electrochemical behavior. In this work, both treatments were found to greatly improve the electrochemical behavior of the porous carbons, cleansing in the case of phenolic-based porous carbons (reticulated vitreous carbon, or RVC, from Energy Research and Generation, Inc., or ERG, Oakland, CA), and particulate additive coating in the case of fiber-based porous carbons (fabricated by SUNY/Buffalo and compared with that which is commercially available from Fiber Materials, Inc., or FMI, Biddeford, ME). An objective of this paper, therefore, is to study the electro-

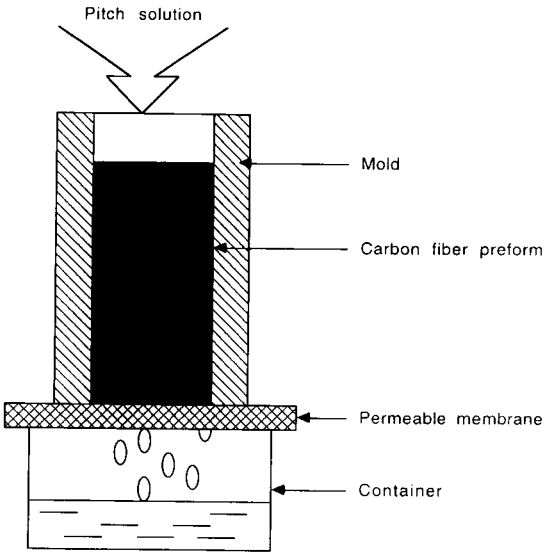

Fig. 1. Set-up for fabricating SUNY fiber-based porous carbons.

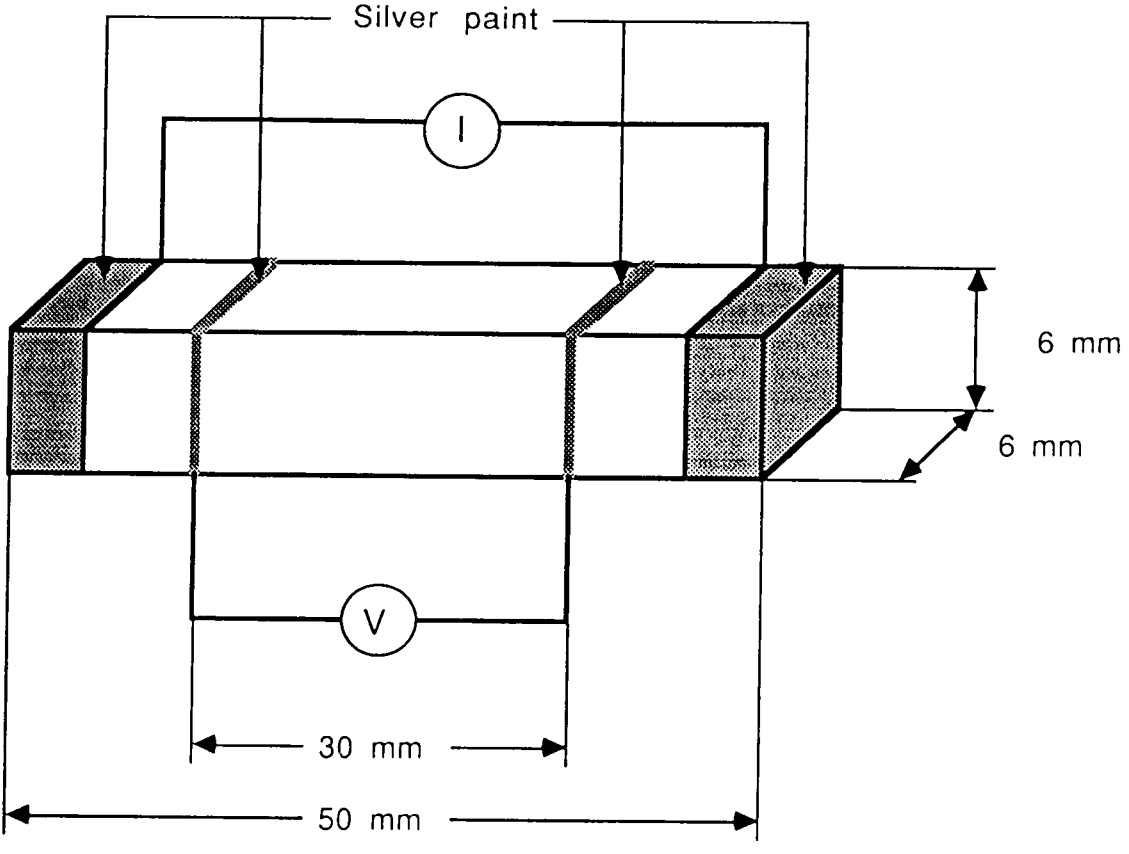

Fig. 2. Set-up for measuring electrical resistivity.

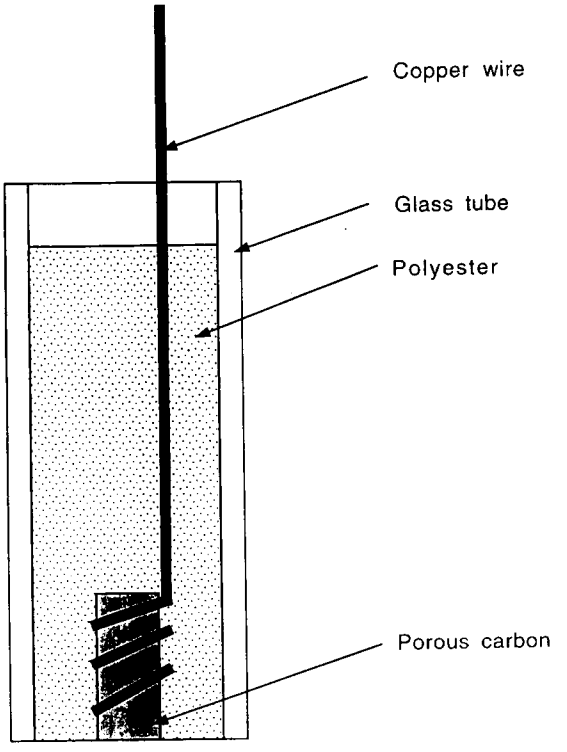

Fig. 3. Cross-section of porous carbon CV electrode.

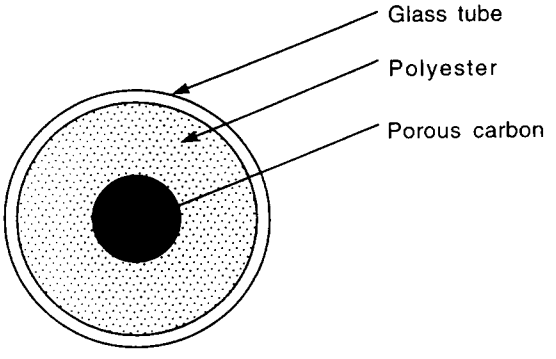

Fig. 4. End view of porous carbon CV electrode.

chemical behavior of porous carbons and the effects of cleansing and carbon particulate addition on the electrochemical behavior. A related objective is to compare the electrochemical behavior of porous carbons made from carbon fibers with those that are made from phenolic. Another related objective is to study the effect of pore density on the electrochemical behavior in the case of porous carbons that are made from phenolic.

For electrochemical applications such as battery and analytical electrodes or capacitors, electrode capacitance is as important a parameter to performance as electrode kinetics. In the former, it is desirable to have a low capacitance in conjunction with a high electron-transfer rate. In the latter, a high capacitance and a high electron-transfer rate is sought. High capacitance is often associated with high surface roughness or high concentration of oxygen-containing surface functional groups, whereas low capacitance is usually due to poor wetting by the electrolyte [21]. Slow capacitive charging has been shown to occur when the electrode displays limited conductivity or exhibits an inhomogeneous surface [21]. It is an objective of this paper then to assess the capacitive behavior of the porous carbons. A related objective is to compare the capacitive behavior of the fiber-based porous carbon with the phenolic-based ones as well as with other carbons conventionally used as electrodes (i.e. carbon paste, carbon black and glassy carbon).

Active electrochemical area is another indicator of the electrochemical performance of materials. For porous materials, the electrochemical area is not necessarily related to the electrode's outer planar area [21]. However, it was implicitly assumed that the electrochemical area is related to the geometric surface area in the design of porous carbons. An objective of this paper is to determine and explain the relationship between the geometric surface area and the active electrochemical area as obtained by cyclic voltammetry (CV) experiments.

There are two classes of commercially available porous carbons; they are carbon fiber based or polymer (usually phenolic) based. In the former, fabrication is accomplished by binding carbon fibers with a carbon-based material (e.g. pitch or phenolic resins, which are subsequently carbonized) [26]. The fiber-based porous carbons may be fabricated to retain flexibility (soft felt) or not (rigid felt), depending primarily on the quantity of binder. This work investigates the rigid version, an example of which is Fiberform from FMI. RVC from ERG is an example of the polymer-based porous carbon (made from a phenolic base). RVC is an open pore, honeycomb "foam" material composed solely of glassy carbon and available in porosity grades from 20 to 500 pores per inch (ppi) [27].

2. EXPERIMENTAL

The FMI fiber-based porous carbon, a rigid, fibrous graphite material (Fiberform), was manufactured by vacuum casting techniques using pitch-based carbon fibers with length to diameter ratios greater than 10:1 and a special high char resin organic binder [26]. The SUNY porous carbon was fabricated from carbon fibers supplied by Ashland Petroleum Company under the trademark Carboflex. The Ashland carbon fibers were short (50, 100, 200 or 400 μm long), 10 μm in diameter, unsized, and pitch-based and had been carbonized at $\sim$1100°C; their properties are shown in Table 1. The pitch used as binder in the SUNY porous carbon was Grade A240, also of Ashland Petroleum Company.

The SUNY porous carbons were fabricated using a five-step process: (i) carbon fiber slurry preparation, (ii) slurry casting, (iii) baking, (iv) impregnation with

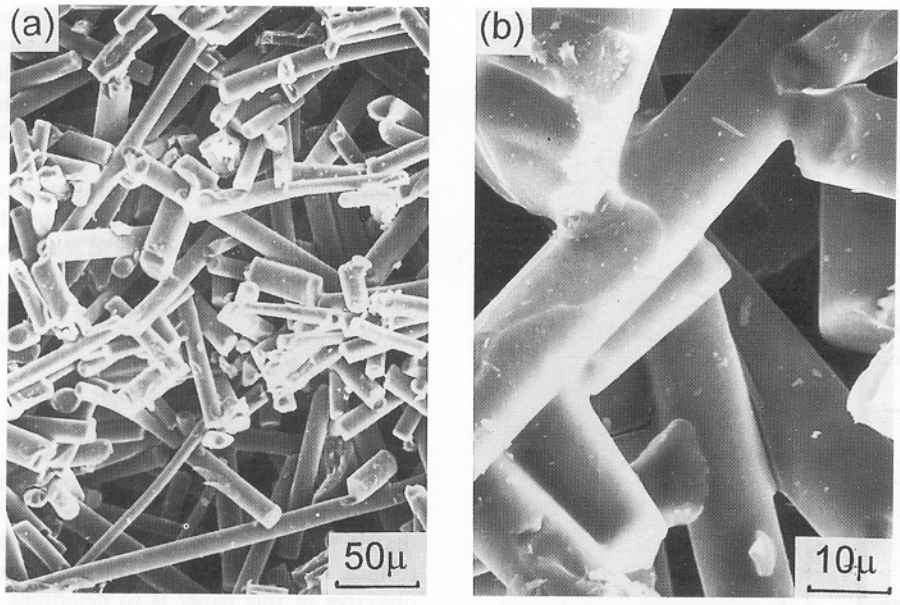

Fig. 5. SEM photographs of SUNY fiber-based porous carbon made with 100 μm long fibers (see text for details).

pitch and (v) carbonization. During slurry preparation, the carbon fibers were dispersed in water containing a surfactant, Triton X-114 (Rohm and Haas, Philadelphia, PA). The slurry was poured into a mold, as shown in Fig. 1, which allowed the excess water to drain. The wet block was removed from the mold and then baked at 85–95°C for 8 hours. The dried block (called a preform) was impregnated with pitch dissolved in methylene chloride, and then air dried for a minimum of 24 hours. Carbonization of the block was achieved by heating in a nitrogen atmosphere at a rate of 10–20°C min^{-1} up to 1000–1200°C, holding for 1 hour and then cooling to room temperature.

Preparation of porous carbons with particulate additives was the same as that described above, except that there were additional steps after step (v). They are: (vi) particulate slurry preparation, (vii) impregnation with slurry of step (vi) into porous carbon obtained in step (v), and (viii) carbonization. Two particulate additives were investigated, carbon black (500 μm mean particle size, Shawinigan acetylene black from Chevron, Houston, TX), and graphite flakes (2 μm wide, 0.5 μm thick, #850 from Asbury Graphite Mills, Inc.). Addition of the carbon black to the porous carbon made of 50 μm long carbon fibers resulted after step (viii) in a 16% increase in the weight compared with the weight after step (v). Addition of graphite flakes to the porous carbon made of 400 μm long carbon fibers increased the weight by 35%.

The volume resistivity of the porous carbons was measured using the four-probe method [28]. The testing set-up is shown in Fig. 2. The porous carbons were shaped into a rectangular bar with the longest axis being the axis of the resistivity measurement. Silver paint in the areas shown in Fig. 2 served as the electrical contacts. The compact's volume electrical resistivity (ρ) was determined as a function of the inner probe separation, l, the cross-sectional area of the sample, A, and the potential drop, ΔV, between the inner probes for a known current flow, I, through the bar, using eqn (1)

$$\rho = (\Delta V/I)(A/l) \tag{1}$$

In the case of the SUNY-fiber-based porous carbons, volume electrical resistivity measurements were made in two directions, namely the direction parallel to the flow during slurry casting (the transverse direction) and the direction perpendicular to the flow (the longitudinal direction). For the FMI-fiber-based porous carbon and the phenolic-based porous carbons, the longitudinal direction corresponded to the direction parallel to the planar surface of the sample, whereas the direction perpendicular to the planar surface (i.e. through the sample thickness) corresponded to the transverse direction.

The compressive strength of the porous carbons was measured by applying a compressive force in the transverse direction to a $10 \times 10 \times 10$ mm cube at a crosshead speed of 1 mm min^{-1}. The compressive strengths of the 100 and 500 ppi phenolic-based porous carbons were impossible to obtain due to their extreme brittleness.

The apparent density of the porous carbons was determined by dividing the weight of a sample by its dimensions. The sample dimensions were measured using a micrometer.

The equation used to determine the specific geometric surface area (SGSA) of the porous carbons was derived from the fiber or strut surface area and the porous carbon volume. For the fiber-based porous carbons:

$$\mathrm{SGSA} = S_f/V_t \tag{2}$$

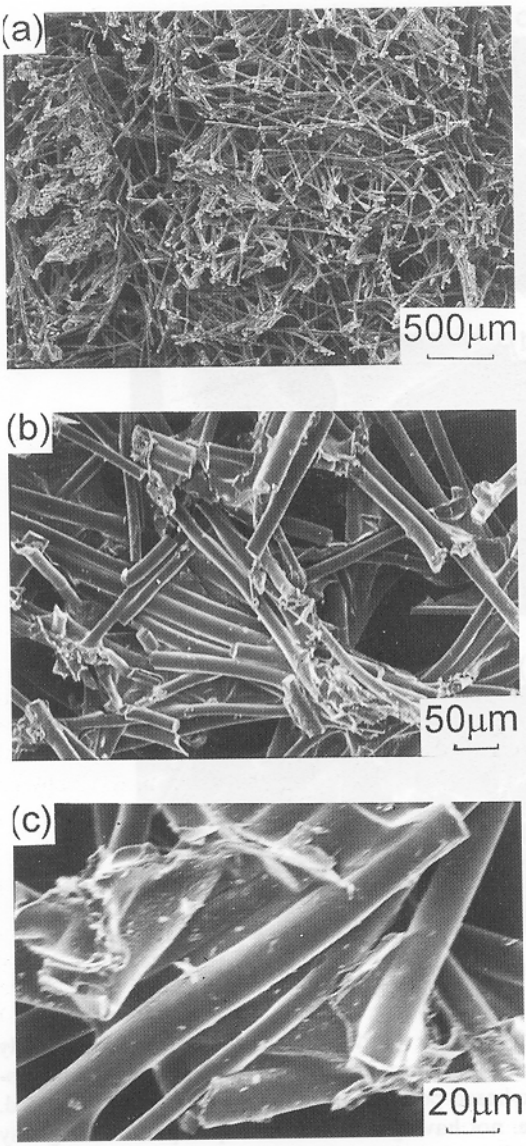

Fig. 6. SEM photographs of FMI fiber-based porous carbon (see text for details).

where S_f = surface area of the fiber and V_t = total volume of the porous carbon.

However,

$$V_f/V_t = \delta_{app}\delta_f \quad (3)$$

where V_f = volume of the fiber, δ_{app} = apparent density and δ_f = density of the fiber.

Therefore,

$$V_t = V_f(\delta_f/\delta_{app}) \quad (4)$$

Substituting for V_t in eqn (2) gives

$$SGSA = (\delta_{app}/\delta_f)(S_f/V_f) \quad (5)$$

Substituting $S_f = 2\pi r\,\mathscr{L}$, and $V_f = \pi r^2\,\mathscr{L}$ into eqn (5) and simplifying gives

$$SGSA = (\delta_{app}/\delta_f)(2/r) \quad (6)$$

where r = the radius of the fiber and $\mathscr{L}$ = the length of the fiber.

Following the same logic, eqn (7), the equivalent of eqn (6), was obtained for the phenolic-based porous carbon, which has struts of rectangular (dimensions L and w) rather than circular cross-sectional shape.

$$SGSA = 2(\delta_{app}/\delta_s)\{(L+w)/(Lw)\} \quad (7)$$

where δ_s = density of the strut L = the length of the strut and w = the width of the strut.

The porous carbon porosity was determined by the equation: $1-(\delta_{app}/\delta_f)$ for the fiber-based porous carbon and $1-(\delta_{app}/\delta_s)$ for the phenolic-based porous carbon. The mean pore size was determined from SEM photographs.

The phenolic-based porous carbon was cleansed by immersing a cut sample into reagent grade methylene chloride contained in a beaker and sonicating for 1 minute using a Branson ultrasonic cleaner. This caused the solvent to change in appearance, from clear to dark, indicating the cleansing action of the medium. The solvent was decanted and submitted for gas chromatography/mass spectroscopy (GC-MS) analysis. The phenolic-based porous carbon was air dried before fabricating into an electrode for CV testing.

Thermogravimetric analysis (TGA) was conducted on the 500 ppi phenolic-based porous carbon using a Perkin-Elmer 7 Series Thermal Analysis System. The gas flow during analysis comprised 30 cc min^{-1} nitrogen mixed with 20 cc min^{-1} air. The temperature was increased at a rate of 10°C min^{-1} to 850°C, and then cooled to room temperature at the same rate. TGA was conducted during heating. After subsequent cooling, CV testing was conducted.

To determine the amount of contaminant on the 100 and 500 ppi phenolic-based porous carbon surfaces, TGA was conducted in nitrogen (flow = 40 cc min^{-1}, though a small amount of air probably remained) using the same Perkin-Elmer system described above. In this case, the temperature was increased at a rate of 20°C min^{-1} to 750°C and then cooled to room temperature at 50°C min^{-1}. TGA was conducted during heating.

The gas chromatography/mass spectroscopy (GC-MS) apparatus used to determine the molecular structure of the material removed during solvent cleansing was a Hewlett-Packard 5972 MSD equipped with a 5890 series II GC. The solvent filtrates were concentrated by evaporating the cleansing medium prior to analysis. The gas chromatograph column was a 30 m × 0.25 mm HP-5 fused silica capillary. One microliter of the concentrated filtrate was injected into the column, held at 50°C for 3 minutes then heated at 10°C min^{-1} to a final temperature of 290°C. The mass spectrometer was operated in the electron impact mode and the sample was scanned from 35 to 550 atomic mass units. The

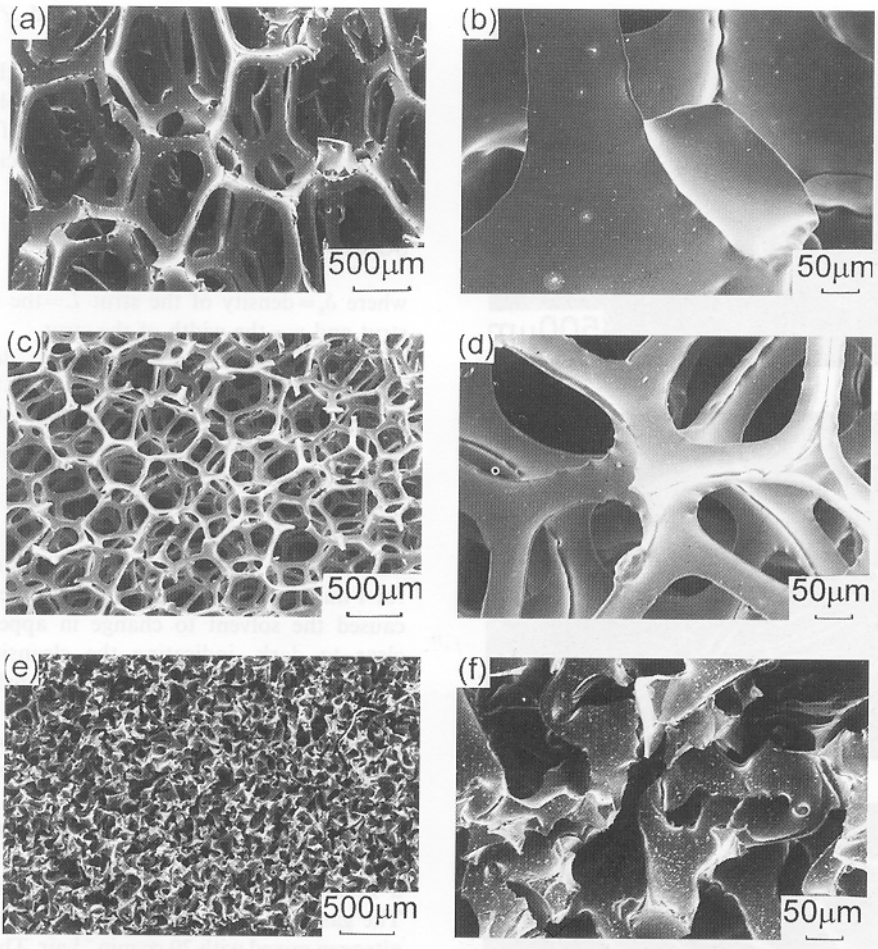

Fig. 7. SEM photographs of phenolic-based porous carbons. (a) and (b) 45 ppi, (c) and (d) 100 ppi, (e) and (f) 500 ppi.

sample spectra were compared with the library spectra to identify components.

Porous carbon electrochemical performance was assessed by cyclic voltammetry (CV) using the same method and set-up as ref. [29]. The porous carbon working electrodes were fabricated in three steps. First, the porous carbon block was cut to size using a cork bore (29.17 mm^2 planar surface area). In the second step, a copper wire (diameter 0.5 mm) was wrapped around the body of the porous carbon to achieve electrical contact and the assembly was inserted into a glass tube. The copper wire protruded from one end of the glass tube and the porous carbon test sample protruded from the opposite end by 0.25 mm. Thirdly, polyester mounting medium was poured into the glass tube containing the wound assembly and allowed to cure. Figure 3 displays a typical electrode configuration. The face of the electrode, 5.7 mm in diameter, is shown in Fig. 4. The CV current densities were calculated by dividing the measured current by the area of the electrode outer surface.

The CV results obtained using the porous carbons were compared with those obtained with glassy carbon, carbon paste and carbon black. Glassy carbon is a hard, solid carbon material, typically known as vitreous carbon. It differs from the phenolic-based porous carbon in that it is not reticulated, i.e. not having a network of open pores. The glassy carbon electrode used in this work was purchased from Bioanalytical Systems (BAS in West Lafayette, IN). The carbon paste (CP 1010), also from BAS, consisted of a mix of Ultra Carbon graphite particles (2–18 μm size, Ultra Carbon from Carbone of America, Bay City, MI) and a paraffin oil binder, while the carbon black (500 μm mean particle size, Shawinigan acetylene black from Chevron, Houston, TX) was mixed with a mineral oil binder. The graphite particle paste (called carbon paste) and carbon black paste electrodes were packed into the cavity of a purchased BAS working electrode holder at a pressure of 10 MPa. The circular electrode outer planar area was 7.92 mm^2.

The rate constant for electron transfer (k_s), the capacitance (C) and the electrochemical area (A) were obtained from the CV data using the method described in ref. [29] in order to evaluate the various porous carbons and their subsequent treatments. In particular, the capacitance was calculated from the current density determined in CV.

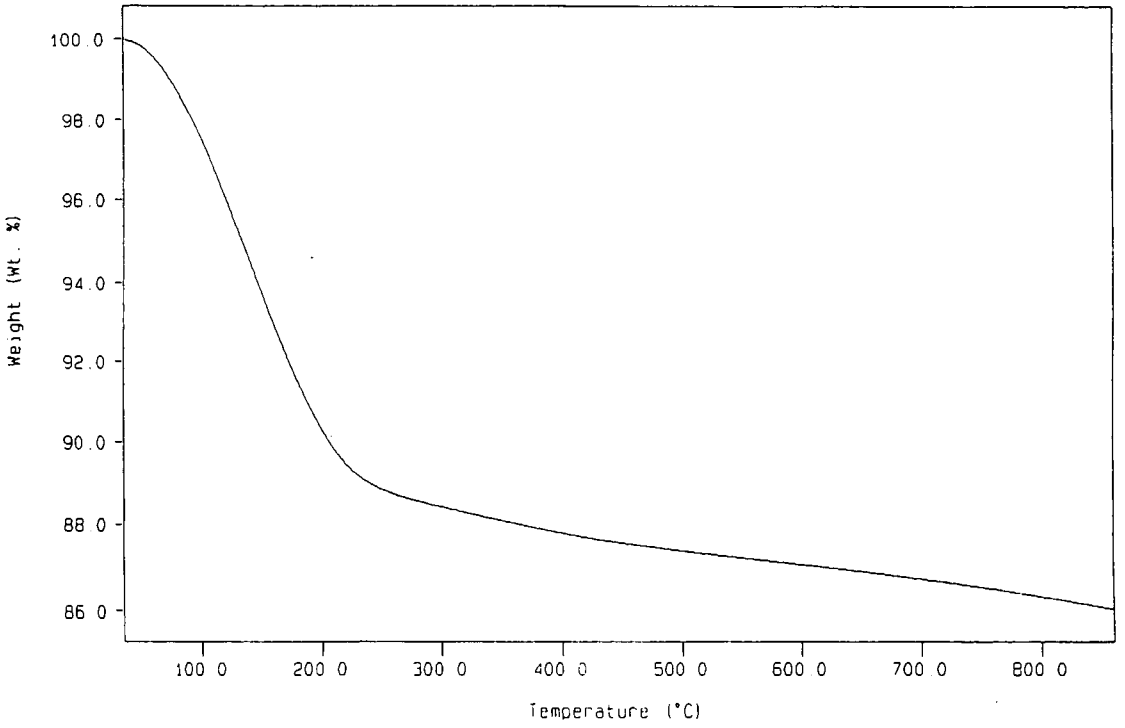

Fig. 8. TGA result during heating of 500 ppi phenolic-based porous carbon in nitrogen.

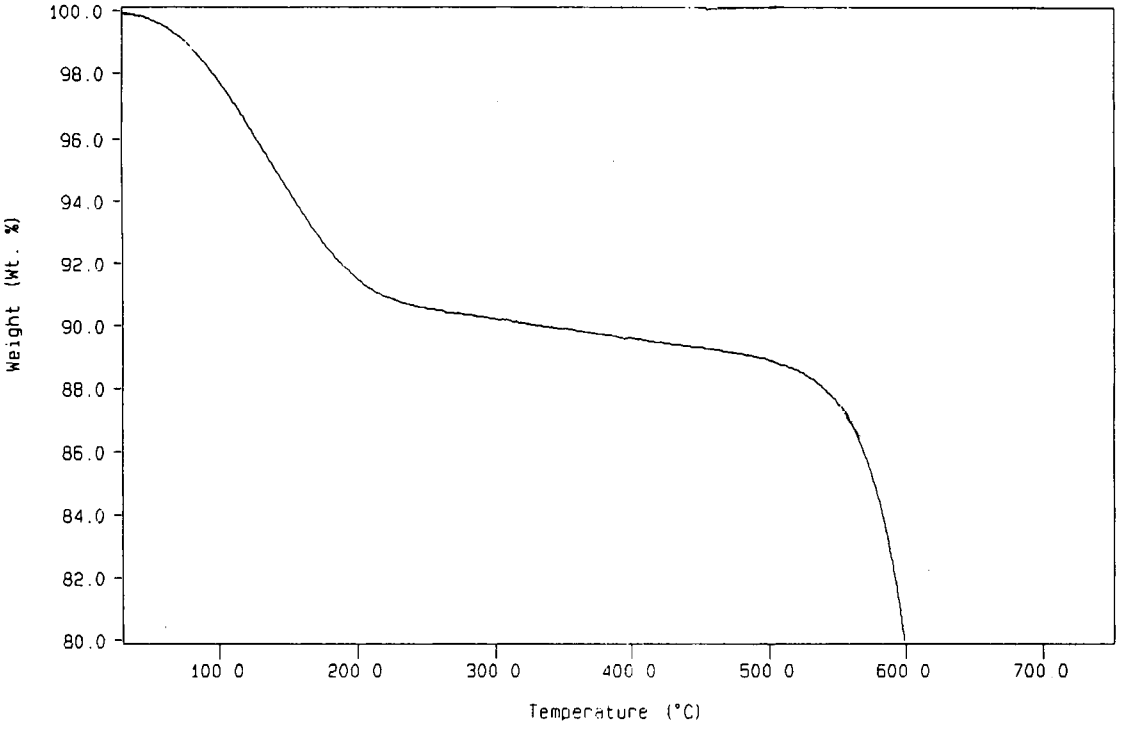

Fig. 9. TGA result during heating of 500 ppi phenolic-based porous carbon in nitrogen plus air.

In order to obtain information related to the wettability of the porous carbon by the electrolyte, the electrolyte absorption capability (absorptivity) and rate of electrolyte absorption were measured by immersing a rectangularly cut sample of the porous carbon in the electrolyte and recording the weight gain as a function of time. A fine wire was threaded to the pores at the surface of the porous carbon, and then shaped into a hook at its end. The hooked wire served two purposes. First, the wire, like a handle,

Table 2. Molecular identifications of contaminants on 500 ppi phenolic-based porous carbon

Molecular weight (amu)	Identification	Chemical formula
152	Acenaphthalene (aromatic)	$C_{12}H_8$
212	Pentadecane (aliphatic hydrocarbon)	$C_{15}H_{32}$
226	Tetradecane	$C_{14}H_{30}$
239	Hexadecane	$C_{16}H_{34}$
253	Octadecane	$C_{18}H_{36}$
278	Dibutyl phthalate[a]	$C_{16}H_{22}O_4$
128	Naphthalene (aliphatic hydrocarbon)	$C_{10}H_8$

[a]Artifact of plastic storage container.

facilitated entry and exit from the electrolyte. Second, the end of the wire, bent in the shape of a hook, suspended the porous carbon sample in the electrolyte during testing. After the porous carbon assemblies were prepared, they were weighed and then immersed in the electrolyte for 15 and 30 seconds and 1, 2, and 5 minutes. At each of these intervals, the wetted assembly was removed from the electrolyte and reweighed. After the weight uptake measurements, the wire was removed from the porous carbon, rinsed in acetone, air dried for 1 minute and then weighed. The porous carbon weight was determined by difference, i.e. the electrode assembly weight minus the wire weight.

The specific electrochemical area was obtained by taking the electrochemical area (A) and dividing by the porous carbon volume exposed to the test solution during CV.

3. RESULTS AND DISCUSSION

The SEM photos in Figs 5–7 show the microstructure of the porous carbons evaluated. The SUNY porous carbon based on fibers is shown in Fig. 5. In the lower magnification view (Fig. 5(a)), the carbon fibers are clearly seen. The higher magnification shows the bonding at the fiber junctions by the carbon binder (based on pitch, Fig. 5(b)). Figure 6 displays the FMI counterpart. The lower magnification view (Fig. 6(a)) shows the binding carbon less well-distributed than that of the SUNY porous carbon (Fig. 5(a)). The FMI binding carbon appears weblike in structure, as shown in the higher magnification view (Fig. 6(b)), collecting a larger quantity of fibers within it compared with the SUNY porous carbon (Fig. 5(b)).

The honeycomb structure characteristic of the phenolic-based porous carbon is clearly seen in the 45 ppi (Fig. 7(a)) and 100 ppi (Fig. 7(c)) samples. The pores of the 500 ppi (Fig. 7(e)) sample, however, are more irregular, not at all resembling a honeycomb. For the 45 ppi (Fig. 7(b)) and 100 ppi (Fig. 7(d)) samples, the phenolic-based porous carbon's struts are essentially rectangular in their planar shape, and are relatively smooth and straight, but decrease in width (the narrow portion of the rectangular shape) as the pore size decreases. The strut widths, as measured from SEM photographs, are: 190 μm for 30 ppi, 110 μm for 45 ppi, 70 μm for 80 ppi and 40 μm for 100 ppi. The 500 ppi (Fig. 7(f)) sample, however, deviates from the rectangular shape in that they are curved, twisted and of varied width (average width = 30 μm). The strut density, given as 1.49 g cm^{-3} [27], is slightly less than that of the fibers used in the SUNY porous carbons (1.6 g cm^{-3}, Table 1), and ~34% lower than that of graphite (theoretical density of 2.25 g cm^{-3}). Some contaminant is observed to be dispersed over the strut surfaces of all three phenolic-based porous carbon samples shown. The heaviest amount of contamination is observed on the 500 ppi struts (clearly visible in Fig. 7(f)). Cleansing in methylene chloride removes the contaminant, as confirmed by SEM. (The contaminant on the 500 ppi sample was no longer visible under SEM after cleansing in methylene chloride.) TGA conducted in nitrogen (Fig. 8) gives the weight loss for the 500 ppi phenolic-based porous carbon. The contaminant was found to comprise 10% of the 500 ppi phenolic porous carbon weight (volatilized up to 225°C). TGA in nitrogen plus air confirms the 10% weight loss (Fig. 9). The TGA results indicate that the contaminant can be volatilized. As both results show, the volatilization occurs mainly between 100 and 200°C. In addition to the information obtained on the contaminant, the TGA in nitrogen plus air provides information on the oxidation characteristics of the 500 ppi phenolic porous carbon. Figure 9 shows that oxidation occurs mainly above about 500°C.

To identify the constituents of the contaminant, GC-MS was conducted on the extract of the 500 ppi phenolic-based porous carbon sample. The 500 ppi sample was selected because it displayed the largest amount of contamination, as indicated by SEM observation (Fig. 7(f)). The major compounds identified (Table 2) were long-chain aliphatic hydrocarbons, with minor components comprising polyaromatic hydrocarbons. Also identified was dibutyl phthalate (molecular weight = 278 g mole^{-1}), an artifact of the plastic storage container.

Table 3 summarizes the mechanical, electrical and structural properties of the porous carbons studied. The SUNY fiber-based porous carbons are consistently more dense and the porosities lower than either the FMI fiber-based porous carbon or the phenolic-

Table 3. Comparison of porous carbon mechanical, electrical and structural properties

	SUNY fiber-based porous carbon (μm)					FMI	Phenolic-based porous carbon (ppi)					
	50	100	200	400	400 with graphite flakes	fiber-basedporous carbon	500	100	80	45	30	20
Apparent density (g cm^{-3})	0.66	0.62	0.43	0.29	0.32	0.18	0.372	0.107	0.091	0.051	0.047	0.047
Porosity (%)	58.8	61.3	73.2	81.8	78.2	95	75.0	92.8	94.4	96.8	97.1	97.1
Volume electrical resistivity ($\Omega \cdot$ cm)												
longitudinal*	0.032	0.041	0.060	0.104	0.092	0.049	–	–	0.467	0.607	0.790	0.682
transverse**	0.051	0.066	0.102	0.233	0.211	0.373	–	–	0.545	0.978	0.918	1.810
anisotropic	1.6	1.6	1.7	2.2	2.3	7.6	–	–	1.2	1.6	1.2	2.7
Compressive strength (MPa)[e]	6.9±0.4	4.8±0.3	1.8±0.1	0.55±0.05	0.91±0.05	0.28	[d]	[d]	0.287±0.01	0.168±0.034	0.113±0.018	0.089±0.004
Mean pore size (μm)	42	50	80	100	95	150	75	110	350	750	900	–
Specific geometric surface area(cm^2 cm^{-3})	1030[a]	968[a]	670[a]	455[a]	735[b]	–	10.95	2.17	1.00	0.45	0.21	–

*Perpendicular to direction of flow during slurry casting for the SUNY porous carbon, and in-plane for the FMI and phenolic-based porous carbons.
**Parallel to direction of flow during slurry casting for the SUNY porous carbon, and through the material thickness for the FMI and phenolic-based porous carbons.
[†]Graphite felt, from ref. [15].
[a]Calculated from the corresponding apparent density by ignoring the contacts between the fibers and ignoring the tips of the fibers.
[b]Calculated by adding the area obtained from the apparent density of the corresponding case without graphite flakes and the area due to the edges of the flakes.
[c]Ratio of transverse resistivity to longitudinal resistivity.
[d]Too brittle for measuring the compressive strength.
[e]In the transverse direction.

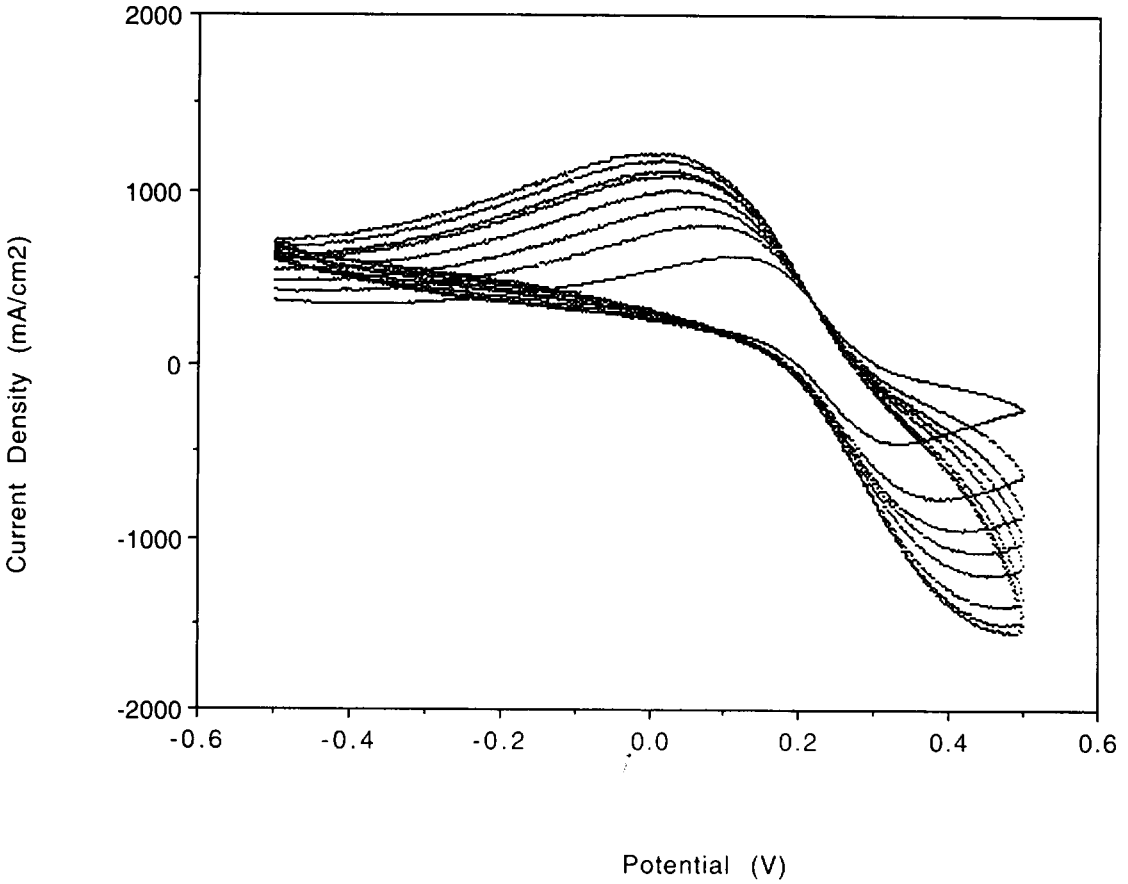

Fig. 10. Cyclic voltammetry results for FM fiber-based porous carbon.

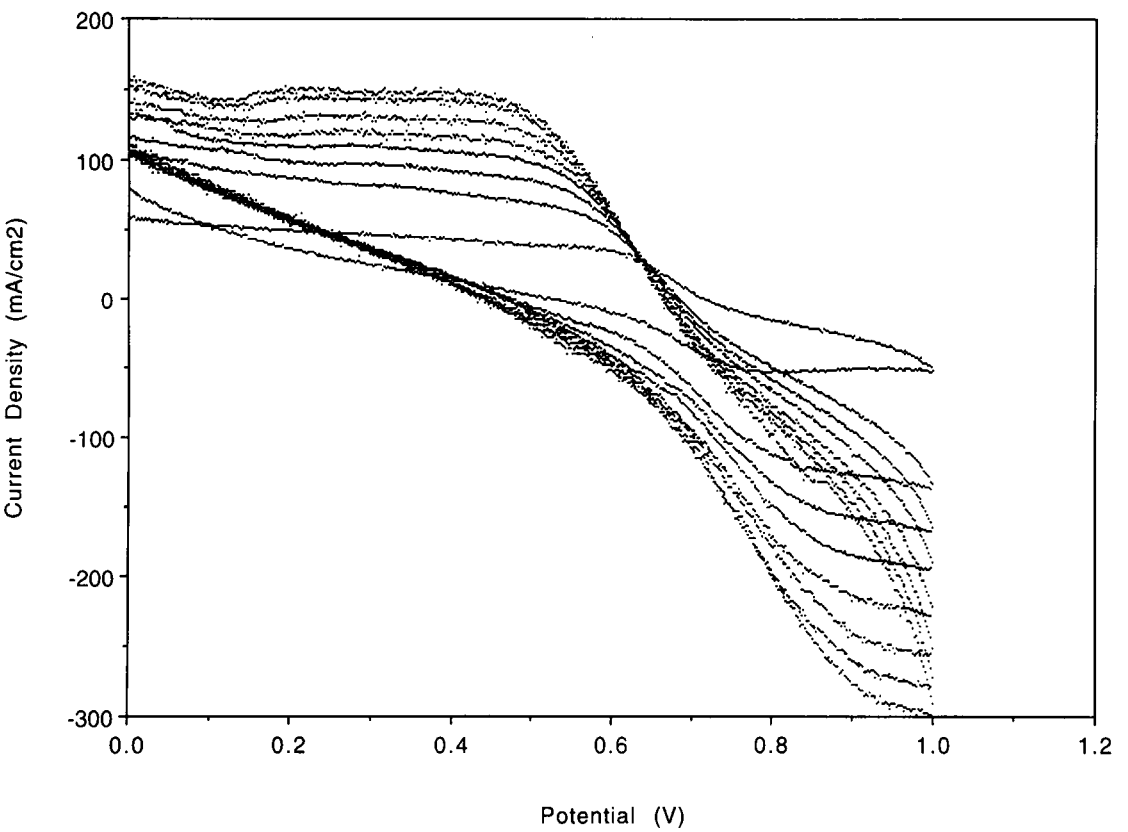

Fig. 11. Cyclic voltammetry results for SUNY fiber-based porous carbon made with 50 μm long fibers.

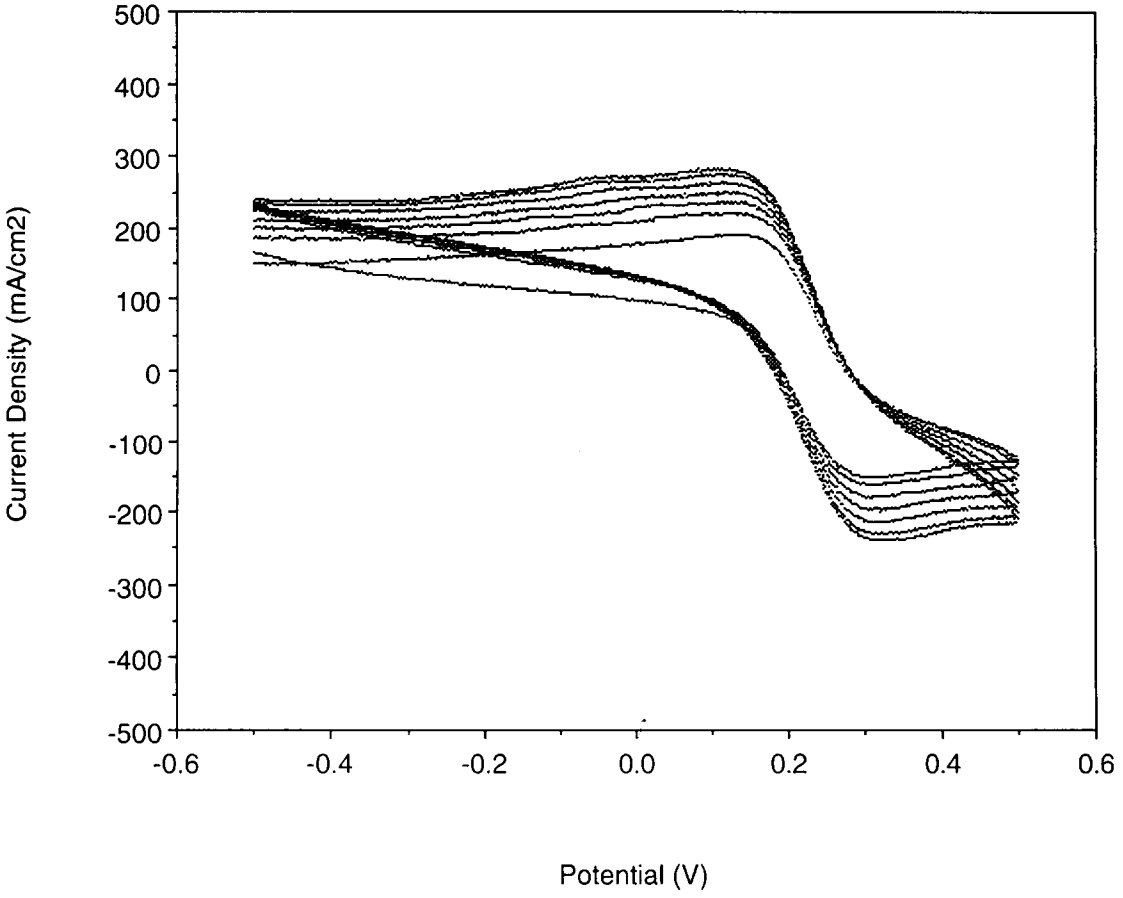

Fig. 12. Cyclic voltammetry results for SUNY fiber-based porous carbon made with 400 μm long fibers.

based porous carbons (all except 500 ppi). The porosity of the SUNY porous carbon, however, increases with increasing fiber length. This is expected since the fibers are bonded at their junctions, allowing almost the complete length of the fiber to form the pore. The higher porosity of the FMI porous carbon, with which the SUNY material is directly comparable, is attributed to the nature in which the carbon binder connects the fibers. In the case of the SUNY porous carbon, the arrangement of the fibers is more random, forming small, finely distributed pores. The fibers in the FMI porous carbon, on the other hand, are more aligned one to another due to the clumping of the fibers by the carbon binder. As shown in Fig. 6(a), the clumping of the fibers in the FMI porous carbon leaves larger pores that are less homogeneously distributed. The effect of the pore structure on the porous carbon's electrical and mechanical properties is evident by the data in Table 3. The FMI porous carbon, with a larger mean pore size (Table 3) and a less evenly distributed pore structure, has a higher electrical resistivity in the transverse direction (i.e. through its thickness) than the SUNY porous carbon and is more anisotropic than the SUNY porous carbon, as shown by the ratio of the transverse resistivity to the longitudinal resistivity. For both FMI and SUNY porous carbons, the resistivity is higher in the transverse direction than the longitudinal direction due to the preferential alignment of the bound fibers in the plane of the longitudinal direction. In addition, the FMI porous carbon has a lower compressive strength than any of the SUNY porous carbons. The SUNY porous carbons, on the other hand, exhibit increasing electrical resistivities and decreasing compressive strengths with increasing fiber lengths. However, the addition of graphite flakes increases the compressive strength. As expected, a higher porosity is associated with a high resistivity. Finally, the mean pore size of the SUNY porous carbons increases and SGSA decreases with increasing fiber length.

The phenolic-based porous carbons exhibit lower apparent density than SUNY as well as FMI fiber-based porous carbons, though the apparent density increases with increasing pore density (in ppi), as shown in Table 3. The porosity of the phenolic-based porous carbons (except for 500 ppi) is higher than that of the SUNY fiber-based porous carbons, but comparable with that of the FMI fiber-based porous carbon; it decreases with increasing pore density. The electrical resistivity of the phenolic-based porous carbon is higher than those of SUNY as well as FMI

Table 4. Porous carbon cyclic voltammetry results obtained at a potential scan rate of 200 mV s^{-1}

Porous carbon	Condition	Anodic peak current density I_a (mA cm^{-2})	Cathodic peak current density I_c (mA cm^{-2})	I_a/I_c	Peak separation, ΔE (mV)
		(±25)	(±25)	(±0.2)	(±10)
Based on carbon fibers					
1: P50	Plain	170	63	2.7	584
2: P50	Plus carbon black	260	191	1.4	168
3: P100	Plain	709	437	1.6	174
4: P400	Plain	319	189	1.7	220
5: P400	Plus graphite flakes	1103	899	1.2	96
6: FMI	As-received	1606	231	6.9	466
Based on graphite flakes					
7: Plain graphite flakes		661	192	3.4	370
Based on phenolic					
8: 30 ppi	As-received	1092	733	1.5	232
9: 45 ppi	As-received	972	652	1.3	200
10: 80 ppi	As-received	1004	474	2.1	298
11: 100 ppi	As-received[a]	583	369	1.6	594
12: 100 ppi	As-received[b]	771	298	2.6	425
13: 100 ppi	As-received[c]	423	189	2.2	302
14: 100 ppi	Methylene chloride cleansed[a]	823	331	2.5	249
15: 100 ppi	Methylene chloride cleansed[b]	841	369	2.3	254
16: 100 ppi	Methylene chloride cleansed[c]	832	356	2.3	244
17: 500 ppi	As-received[d]	2492	1258	2.0	214
18: 500 ppi	Methylene chloride cleansed[d]	2243	1893	1.2	96
19: 500 ppi	TGA (N_2+air)[d]	883	661	1.3	176
20: 500 ppi	TGA (N_2)[d]	1935	199	5.2	356
Other carbons					
21: Carbon paste		975	704	1.4	222
22: Glassy carbon		1213	1040	1.2	122
23: Carbon black		9000	8297	NA	NA

[a]Batch a; [b]batch b; [c]batch c; [d]batch d; [e]indeterminable due to the irreversible CV response (absence of peaks).

Table 5. Electrochemical behavior of porous carbon (sample numbers correspond to those of Table 4)

Porous carbon	Condition	k_s (cm s^{-1}) ±0.0002	Capacitance* (μF cm^{-2}) ±0.05	Electrochemical area† (cm^2) ±5
Based on carbon fibers				
1: P50	Plain	Irreversible	0.42	58
2: P50	Plus carbon black	0.0054	0.60	15
3: P100	Plain	0.0050	1.28	30
4: P400	Plain	0.0023	1.05	24
5: P400	Plus graphite flakes	0.0095	0.75	9
6: FMI	As-received	Irreversible	3.00	121
Based on graphite flakes				
7: Plain graphite flakes		Irreversible	1.91	17
Based on phenolic				
8: 30 ppi	As-received	0.0016	1.87	442
9: 45 ppi	As-received	0.0035	1.46	252
10: 80 ppi	As-received	Irreversible	2.20	286
11: 100 ppi	As-received[a]	Irreversible	1.58	109
12: 100 ppi	As-received[b]	Irreversible	1.39	121
13: 100 ppi	As-received[c]	Irreversible	0.81	41
14: 100 ppi	Methylene chloride cleansed[a]	0.0005	1.74	70
15: 100 ppi	Methylene chloride cleansed[b]	0.0004	1.84	84
16: 100 ppi	Methylene chloride cleansed[c]	0.0009	1.74	70
17: 500 ppi	As-received[d]	0.0027	2.55	86
18: 500 ppi	Methylene chloride cleansed[d]	0.0133	2.08	84
19: 500 ppi	TGA (N_2+air)[d]	0.0049	1.11	24
20: 500 ppi	TGA (N_2)[d]	Irreversible	1.82	48
Other carbons				
21: Carbon paste		0.0023	2.43	27
22: Glassy carbon		0.0090	1.56	17
23: Carbon black		Irreversible	27.50	431

*Per unit outer planar area; †outer planar area = 0.0792 cm^2; [a]batch a; [b]batch b; [c]batch c; [d]batch d.

Table 6. Electrolyte absorptivity and rate of electrolyte absorption for as-received porous carbons

Porous carbon type	Electrolyte absorption (g electrolyte/g carbon) ±0.5	Rate of electrolyte absorption (g electrolyte/g carbon in 15 seconds) ±0.5
Fiber-based		
SUNY 400 μm	3.4	11.6
SUNY 400 μm plus graphite flakes	2.1	6.1
FM1	1.4	4.3
Phenolic-based		
100 ppi	6.1	14.6
500 ppi	1.5	1.0

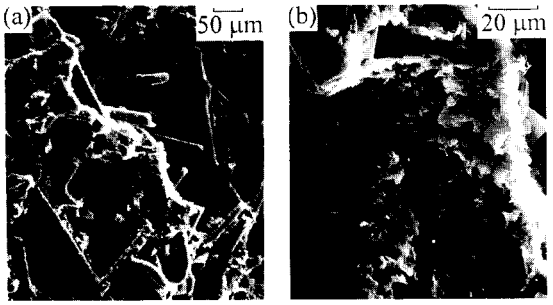

Fig. 13. SEM photograph of SUNY fiber-based porous carbon made with 400 μm long fibers and graphite flakes.

fiber-based porous carbons, whether in longitudinal or transverse directions. Both fiber-based porous carbons and phenolic-based porous carbons have the resistivity lower in the longitudinal direction than the transverse direction. The resistivity anisotropy in the phenolic-based porous carbon is attributed to the anisotropic pore shape, i.e. the preferential orientation of the struts in the plane of the longitudinal direction. In other words, the layers of pores are closer together than the distances between struts created by the pore sizes. The compressive strength of the phenolic-based porous carbons decrease with decreasing pore density, even though strut lengths and widths increase with decreasing pore density.

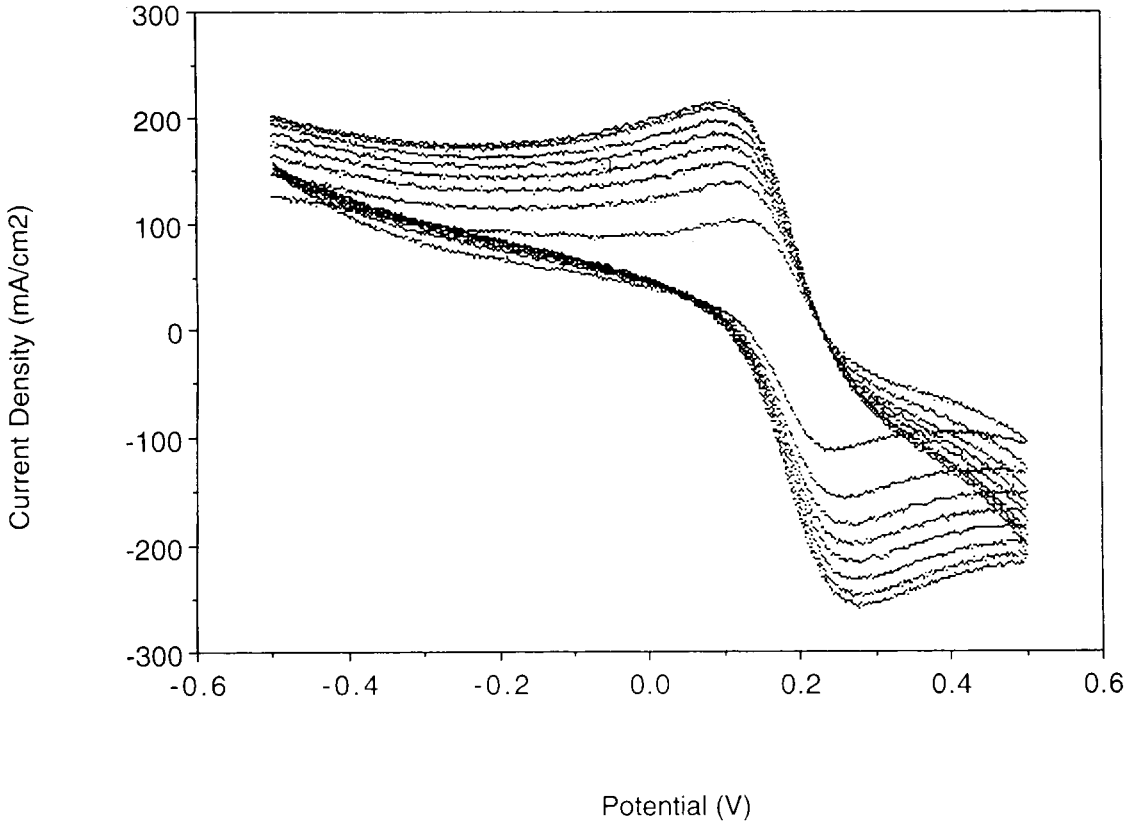

Fig. 14. Cyclic voltammetry results for SUNY fiber-based porous carbon made with 50 μm long fibers and carbon black.

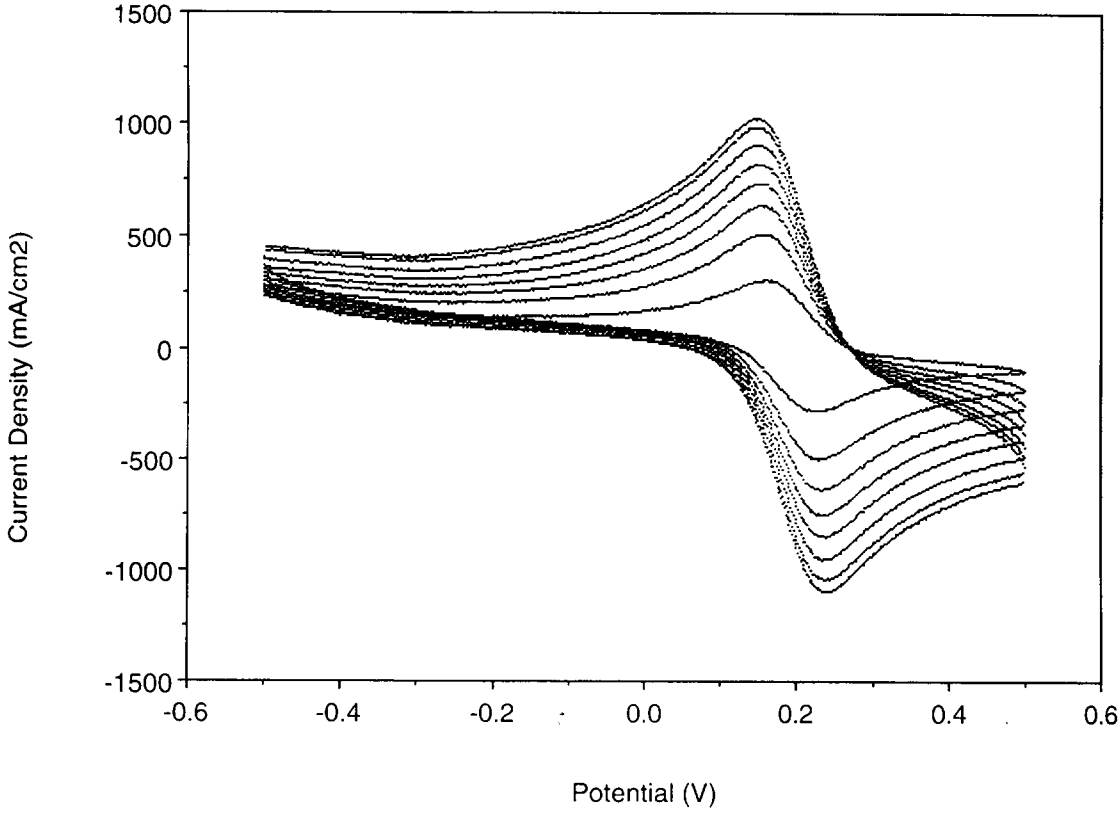

Fig. 15. Cyclic voltammetry results for SUNY fiber-based porous carbon made with 400 μm long fibers and graphite flakes.

This is because the apparent density decreases and the mean pore size increases with decreasing pore density. Along with an increase in the mean pore size is a decrease in SGSA, as expected.

The CV plots of the fiber-based porous carbons are shown in Figs. 10–12. All three types of such carbons demonstrate poor reversibility. The FMI porous carbon (Fig. 10) exhibits higher anodic current density capability, C and A than any of the SUNY porous carbons (Tables 4 and 5), including those shown in Fig. 11 (made with 50 μm length fibers) and Fig. 12 (made with 400 μm length fibers). The electrolyte absorptivity and rate of absorptivity (Table 6) are much higher for the SUNY porous carbon made with 400 μm length fibers compared with the FMI porous carbon, so the higher current density capability of the FMI porous carbon is attributed to the microstructure and not to the electrode wetting characteristics. The FMI porous carbons have a different binder and are joined by clumping of the fibers within the binder, whereas the SUNY porous carbon involves carbon fibers that are joined at their ends by the binder. The clumping by the binder probably allows more contact points between the fibers to facilitate electron flow. Supporting this thought is that the FMI porous carbon displays much lower longitudinal (in-plane) electrical resistivity compared with the transverse electrical resistivity – a characteristic not seen with the SUNY porous carbons. Moreover, the clumping of the fibers in the FMI porous carbon results in a less uniform pore structure and larger pores compared with the SUNY porous carbons (Fig. 6 compared with Fig. 5). The consequent roughness of the electrode's outer planar surface contributes to increasing the capacitance [21].

Of the three SUNY fiber-based porous carbons without additives (samples 1, 3 and 4, Tables 4 and 5), the type made with 100 μm long fibers demonstrates best electrochemical behavior (the highest k_s). This is believed to be due to a synergy achieved by a combination of properties. The porous carbon made with the 100 μm long fibers has low electrical resistivity (compared with the porous carbon made with 400 μm fibers), high porosity (compared with the porous carbon made with 50 μm fibers) and high SGSA (compared with the porous carbon made with 400 μm fibers), all of which contribute to its better electrochemical performance.

Since particle-to-particle connectivity influences electrical properties, electrochemical properties, which depend on electrical conduction within the electrode as well as electron transfer across the electrode–electrolyte interface, are expected to be improved by this connectivity. Carbon particulates, like carbon black or graphite particles, are used to enhance electrical conduction in materials of high resistivity (for example, battery cathodes). Therefore,

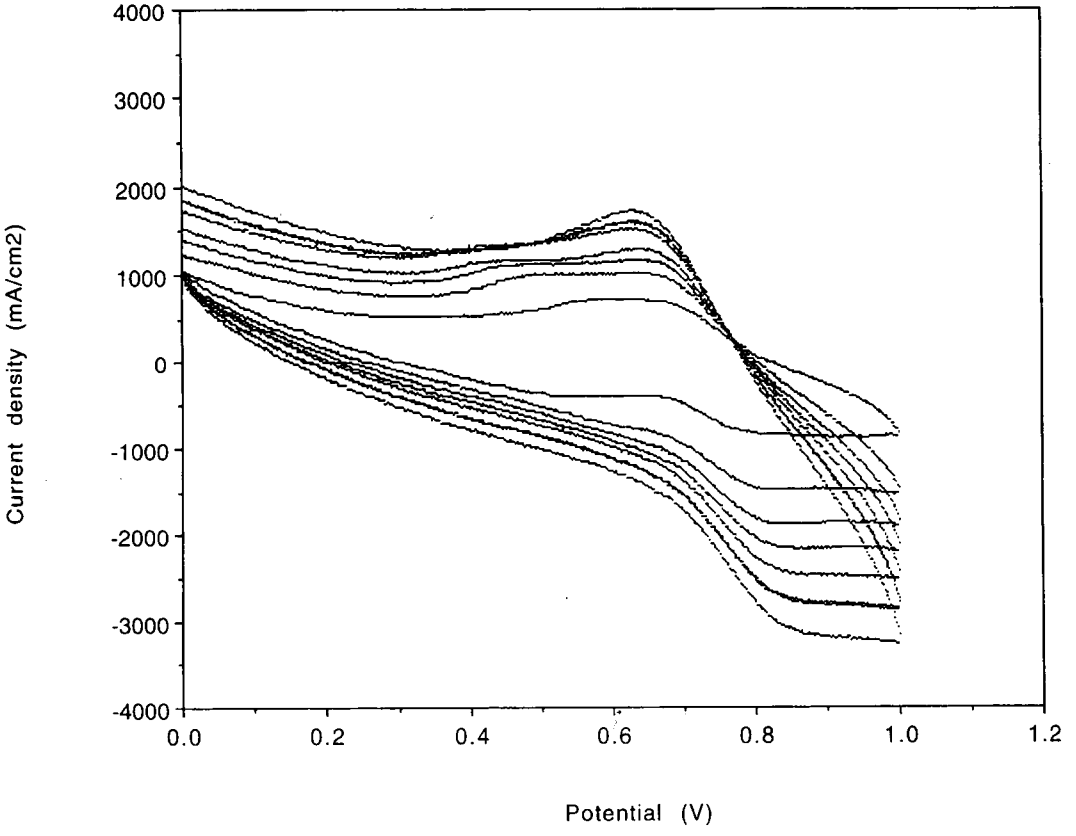

Fig. 16. Cyclic voltammetry results for graphite flakes.

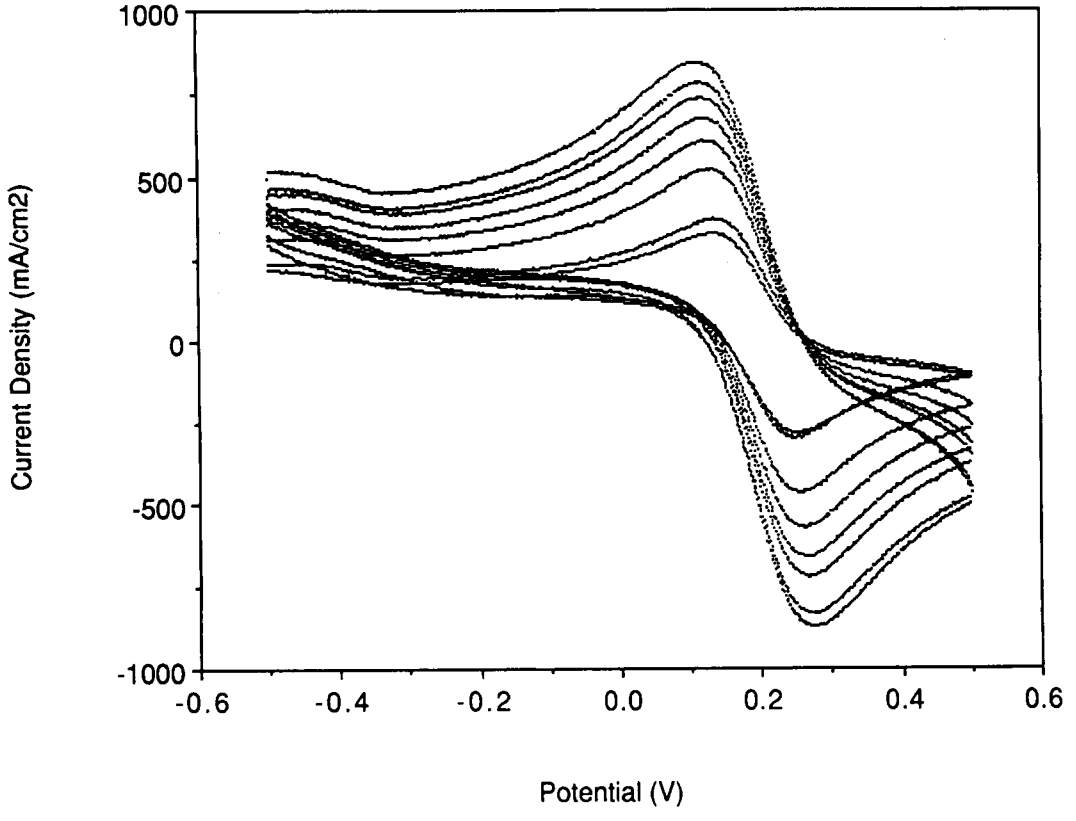

Fig. 17. Cyclic voltammetry results for carbon paste.

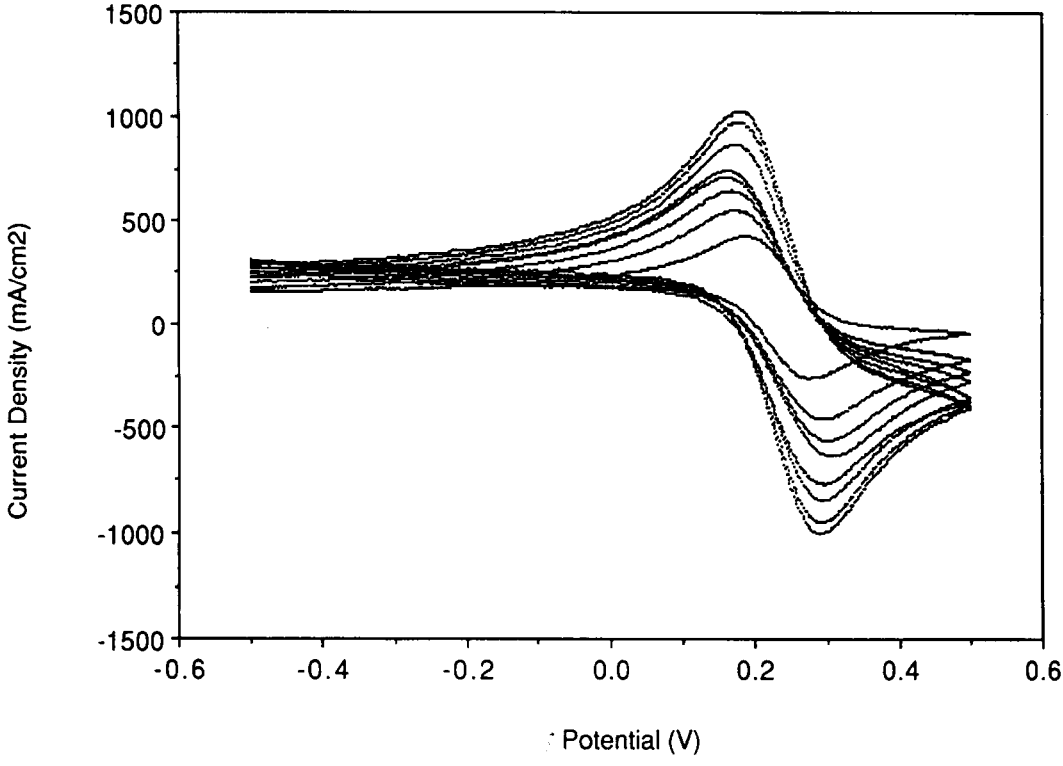

Fig. 18. Cyclic voltammetry results for glassy carbon.

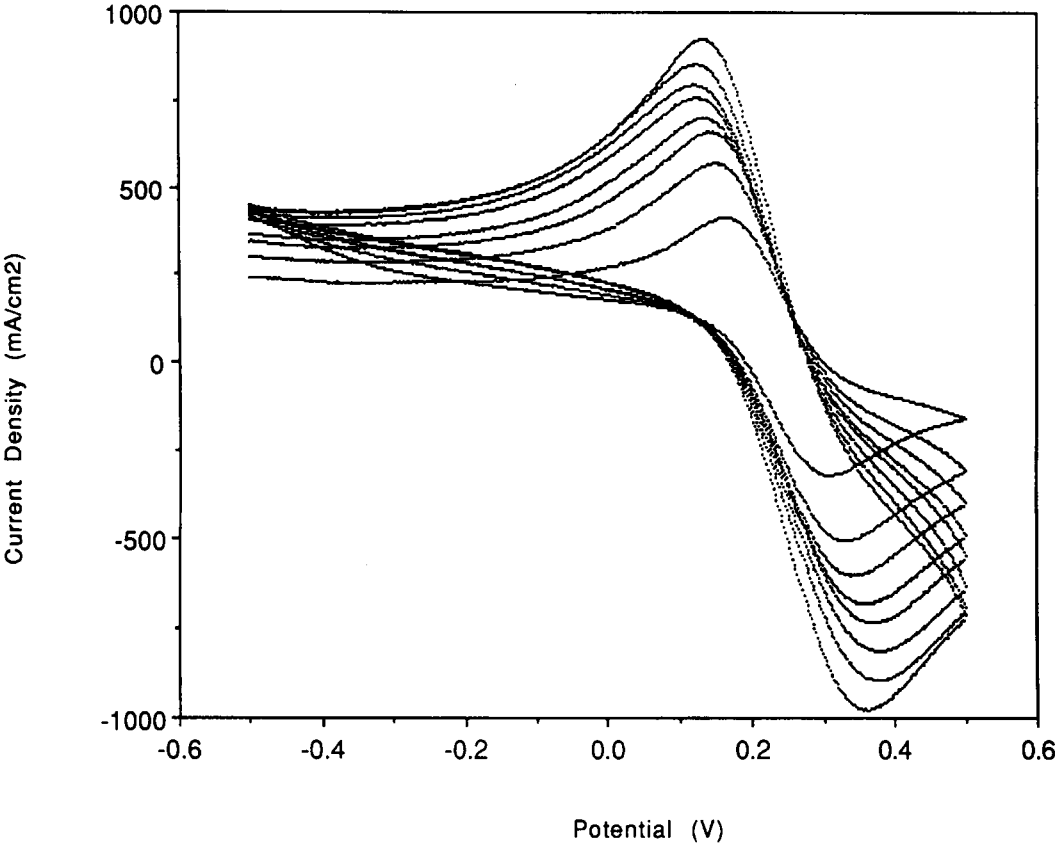

Fig. 19. Cyclic voltammetry results for 30 ppi phenolic-based porous carbon.

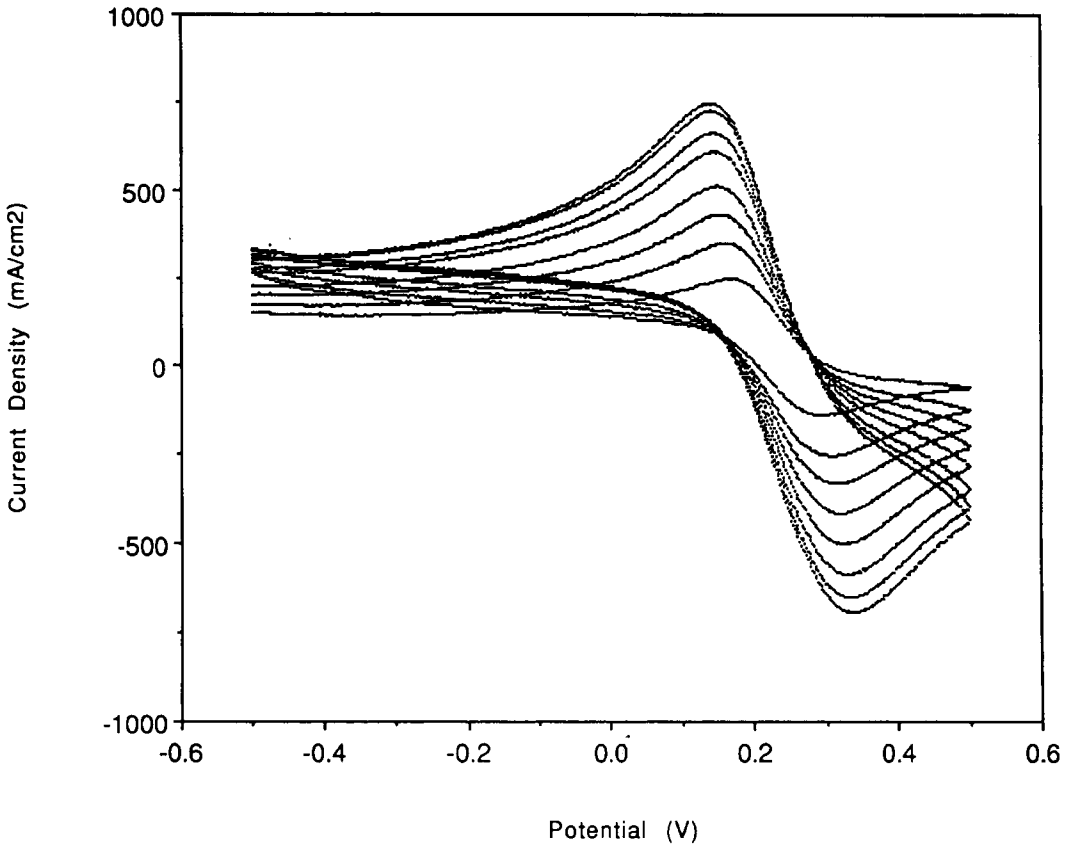

Fig. 20. Cyclic voltammetry results for 45 ppi phenolic-based porous carbon.

various carbons were added to the SUNY fiber-based porous carbons in order to enhance the porous carbon electrical properties. By coating the carbon fibers with the carbon particulate, better electrical connectivity within the porous carbon was expected. Additionally, the porous carbon electrode surface area was also expected to be increased by the additives. Carbon black (mean particle diameter of 420 Å) was added to the porous carbon made with the 50 μm long fibers, increasing its weight by 16%, whereas, graphite flakes (2 μm wide) were added to the porous carbon made with 400 μm long fibers, increasing its weight by 35%. In both cases, the carbon particulate additives increase the porous carbon current density capability (Table 4), as well as the porous carbon electrode kinetics (k_s in Table 5). Quasi-reversibility is achieved using carbon black and the 50 μm long fibers with redox peak separations measured at 168 mV (sample 2, Tables 4 and 5). Better reversibility is observed when the 2 μm wide graphite flakes were added to the 400 μm fiber slurry (sample 5, Tables 4 and 5). As shown in Table 4, a 96 mV redox peak separation is realized, indicating fast electron exchange at this porous carbon working electrode. Peak separation is also observed to be independent of the scan rate. The electron-transfer rate constant k_s (Table 5) is the highest for this composite fiber-based porous carbon, confirming improved kinetics. The effect on current density capability is greater for the graphite additive to the 400 μm long carbon fiber porous carbon compared with the carbon black additive to the 50 μm long carbon fiber porous carbon. For the porous carbon made with 400 μm long carbon fibers, the porosity is little affected by the graphite flake addition (Table 3), while the electrical resistivity is slightly reduced (Table 3), and the electrolyte absorptivity and absorption rate are decreased by about 30% (Table 6); the SGSA (Table 3), however, is substantially increased (about 50%) and is the main cause for the improved electrochemical behavior. Figure 13 shows the microstructure of the SUNY porous carbon made with the 400 μm long fibers coated with graphite flakes. The coating is particulate in appearance and is not uniform on all the fibers. The graphite flakes (2 μm in diameter) primarily lie on the surface of the fibers (10 μm in diameter), such that the large area of the flake is parallel to the fiber surface. However, a portion of the flakes reside between adjacent fibers. Figures 14 and 15 graphically show the improved electrochemical performance of the porous carbons with the additives.

The electrochemical performance of the 400 μm long fiber and graphite flake composite porous carbon is superior to both of its individual constituents, as shown by comparing Fig. 12 (plain 400 μm

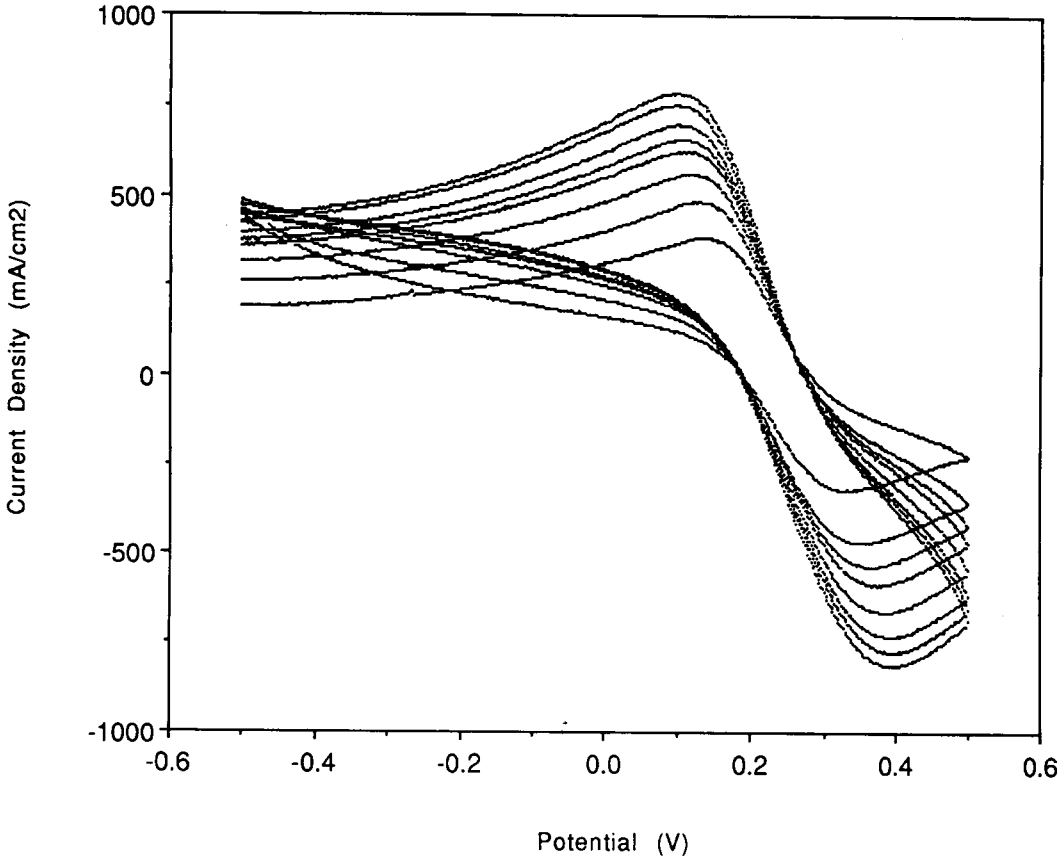

Fig. 21. Cyclic voltammetry results for 80 ppi phenolic-based porous carbon.

porous carbon, sample 4, Tables 4 and 5) and Fig. 16 (plain graphite flakes, sample 7, Tables 4 and 5) with Fig. 15 (the 400 μm long fiber and graphite flake composite, sample 5, Tables 4 and 5). In fact, the graphite-flake carbon fiber composite porous carbon also performs better than conventional carbon paste and glassy carbon (respectively, Figs. 17 and 18, samples 21 and 22 of Tables 4 and 5).

Figures 19–23 display the CV plots for phenolic-based porous carbons of various pore densities (in ppi). The corresponding CV data are listed in Tables 4 and 5. In general, the phenolic-based porous carbons tend to display higher current density capability and better reversibility than the plain (without additive coating) fiber-based porous carbons. In particular, the 500 ppi porous carbon (as-received or methylene chloride cleansed) gives the greatest current density capability among all porous carbons studied. This high current density capability is not associated with a high electrolyte absorption or a high rate of electrolyte absorption (Table 6), so it is not due to electrolyte wettability, but is due to connectivity within the porous carbon microstructure, which has numerous and broad strut junctions (Figs 7(e) and (f)).

Three batch runs of the 100 ppi phenolic-based porous carbon were assessed, and all three display irreversible electrochemical performance with varying CV outputs, as shown in Table 4. The batch-to-batch variation of the electrochemical performance is attributed to the varying degree of cleanliness, as depicted by particulate contaminants on the surface of its struts. TGA in nitrogen determined the contaminant levels to be 8% (sample 11, Tables 4 and 5), 1% (sample 12, Tables 4 and 5) and 12% (sample 13, Tables 4 and 5) for the three batches. A lower contaminant level is associated with a higher electrochemical area (Table 5) and a greater current density capability (Table 4). This indicates that the contaminant is harmful to the electrochemical response. However, the capacitance (Table 5) shows no correlation with the amount of contaminant, probably due to the variation in contaminant molecular structure.

Since, in a previous study [29], methylene chloride was found to be effective in the removal of carbon filament surface contaminants, the three batches of 100 ppi phenolic-based porous carbon (labeled 14, 15 and 16 in Tables 4 and 5; 14 was obtained by cleansing 11, 15 was obtained by cleansing 12, 16 was obtained by cleansing 13) were cleansed using methylene chloride. After cleansing, the particulate surface contaminant is absent and CV results (Tables 4 and 5, Fig. 24) demonstrate more consistent (from batch-to-batch) C and A, and the irreversible redox reaction is changed to being quasi-reversible with some measure of k_s. Moreover, the 500 ppi

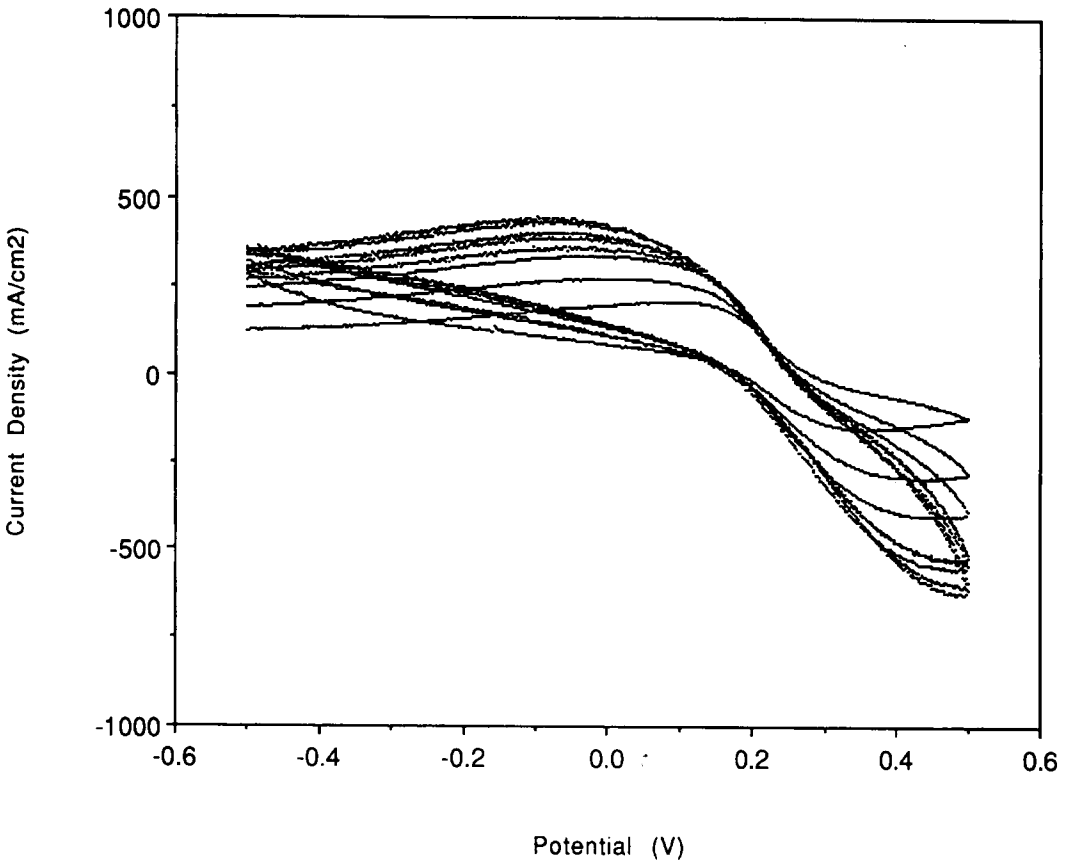

Fig. 22. Cyclic voltammetry results for 100 ppi phenolic-based porous carbon.

sample subjected to TGA in nitrogen plus air up to 850°C (sample 19 in Tables 4 and 5 and Fig. 25) gives higher k_s than the as-received sample (sample 17 and Fig. 23) and than the sample that had been subjected to TGA in nitrogen (sample 20 and Fig. 26), though a lower k_s than the methylene chloride cleansed sample (sample 18 and Fig. 24). The higher k_s for sample 19 than samples 20 and 17 is attributed to oxygen-containing functional groups [22]. Additionally, cleansing or heating in nitrogen results in higher C and A, compared with that achieved by heating in nitrogen plus air (Fig. 25). The low C obtained after heating in nitrogen plus air is associated with low current density capability (used to compute C), which is due to the microstructural effect of weight loss during oxidation (Fig. 9). The difference in k_s obtained by cleansing and heating is probably due to the formation of different surface functional groups. In the case of methylene chloride cleansing, chlorine-containing groups may form, whereas, in the case of heating in nitrogen plus air, oxygen-containing groups may form. In the case of heating in nitrogen, nitrogen-containing groups may form. For methylene chloride cleansing, the effect is greater on k_s compared with heating in nitrogen plus air (Table 5), suggesting the importance of chlorine-containing functional groups over oxygen-containing functional groups. In the nitrogen heating case, the effect is detrimental on k_s (Table 5), in spite of the contaminant removal, indicating the importance of the functional groups.

Removing the hydrocarbon contaminants on the phenolic-based porous carbons results in reproducible and enhanced CV behavior. In a previous study using carbon filaments of diameter 0.1 μm [29], it was found that hydrocarbon contaminants on the filaments were introduced during the fabrication process and removal of the contaminants by methylene chloride cleansing increased k_s. It is believed that the phenolic-based porous carbon fabrication process is also the source of the hydrocarbon surface contaminants. In the case of carbon filaments, contaminant removal increases k_s, mainly because of the increased packing density of the filament electrode [29]. In the case of phenolic-based porous carbons, contaminant removal increases k_s not because of a change in the packing density, but because of a change in surface chemistry. In particular, oxygen-containing functional groups on the original surface of the carbon are known to enhance the electrochemical behavior [21,22] and this effect of contaminant removal by solvent cleansing has been observed in the case of carbon filaments [29]. After methylene chloride cleansing of the 500 ppi phenolic-based porous carbon, k_s is even higher than that achieved with the fiber-based porous carbon coated with graphite

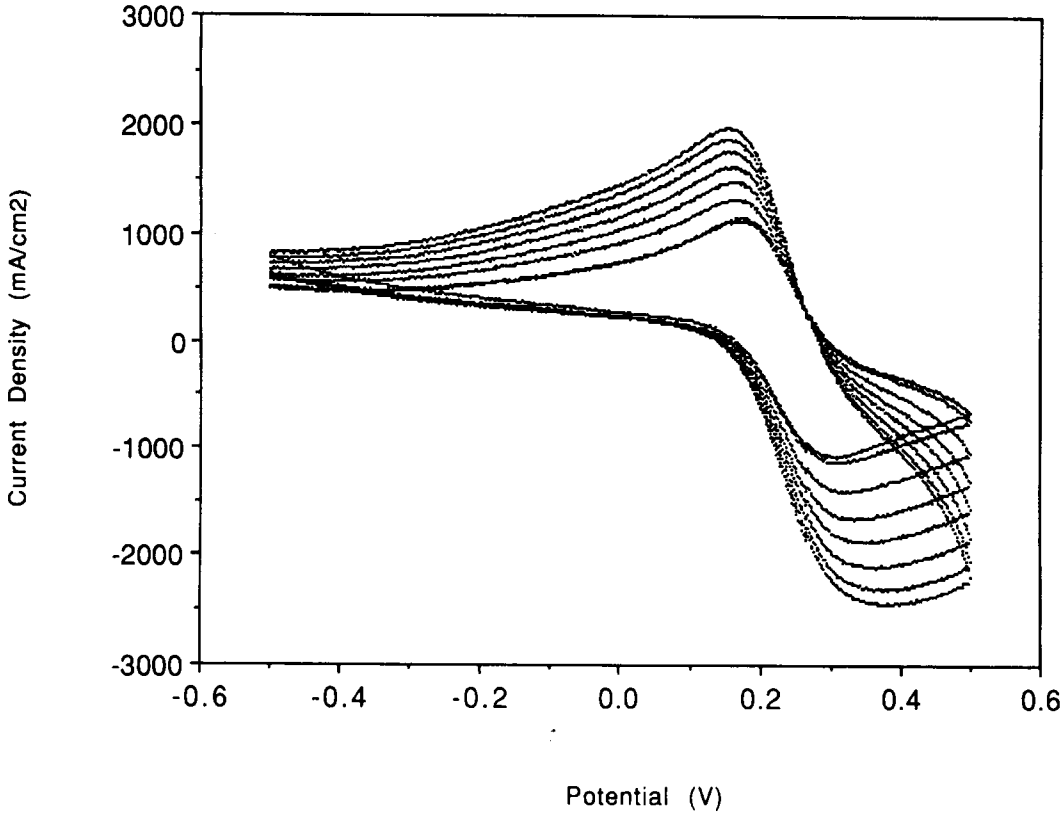

Fig. 23. Cyclic voltammetry results for 500 ppi phenolic-based porous carbon.

flakes, and markedly higher than its uncleansed version.

Porous carbons were intuitively thought to increase in active electrochemical area as the geometric surface area increased. Table 7 shows that this is wrong in most cases. Table 7 compares SGSA (area per unit volume) with the electrochemical area and the specific electrochemical area (area per unit volume) as determined from CV. In the case of the plain fiber-based porous carbons, when SGSA decreases (as fiber length increases), the electrochemical area and the specific electrochemical area were also found to decrease (compare samples labeled 1, 3 and 4 in Table 7), in agreement with the intuitive thought. However, addition of graphite flakes further decreases the electrochemical and specific electrochemical areas (compare samples 4 with 5 in Table 7), while SGSA increases, in contrast to the intuitive thought; the former is attributed to the lower kinetic activity (i.e. irreversible k_s) of the graphite particle additive (sample 6 in Table 5), while the latter is due to the area associated with the graphite flake edges. In particular contrast to intuitive thought is the behavior of the phenolic-based porous carbons, for which an increase in SGSA (an increase in the pore density in ppi) is associated with a decrease in the electrochemical area and a rather constant specific electrochemical area. (The only exception to this is that the 100 ppi phenolic-based porous carbon exhibits a slightly lower electrochemical area than the 500 ppi phenolic-based porous carbon, probably due to a difference in morphology of the phenolic-based porous carbon struts. Whereas the struts of the 100 ppi phenolic-based porous carbon (as for 80, 45 and 30 ppi) are relatively straight and smooth, those of the 500 ppi are curved and twisted. Furthermore, the 500 ppi struts are shorter than those of the 100 ppi version, providing a larger number of broad strut junctions ($\sim 100\ \mu$m broad) than the 100 ppi sample. The tortuosity and larger number of broad strut junctions of the 500 ppi phenolic-based porous carbon increase the specific geometric surface area, which, in turn, increases the electrochemical area.) This is believed to be due to the penetrability of the porous carbon by the electrolyte. A smaller pore size (i.e. a larger pore density, as for 500 ppi compared with 100 ppi), even though associated with a higher SGSA (Table 7), limits the absorption of electrolyte within the body of the porous carbon (Table 6), which, in turn, affects the electrochemical activity of the porous carbon itself. With respect to the specific electrochemical area per unit volume, similar magnitudes were obtained regardless of the pore density (ppi), because the specific electrochemical area depends on both SGSA and the electrochemical area, which vary with the pore density (ppi) in opposite directions. The highest electrochemical area, which is even higher than that obtained using carbon black,

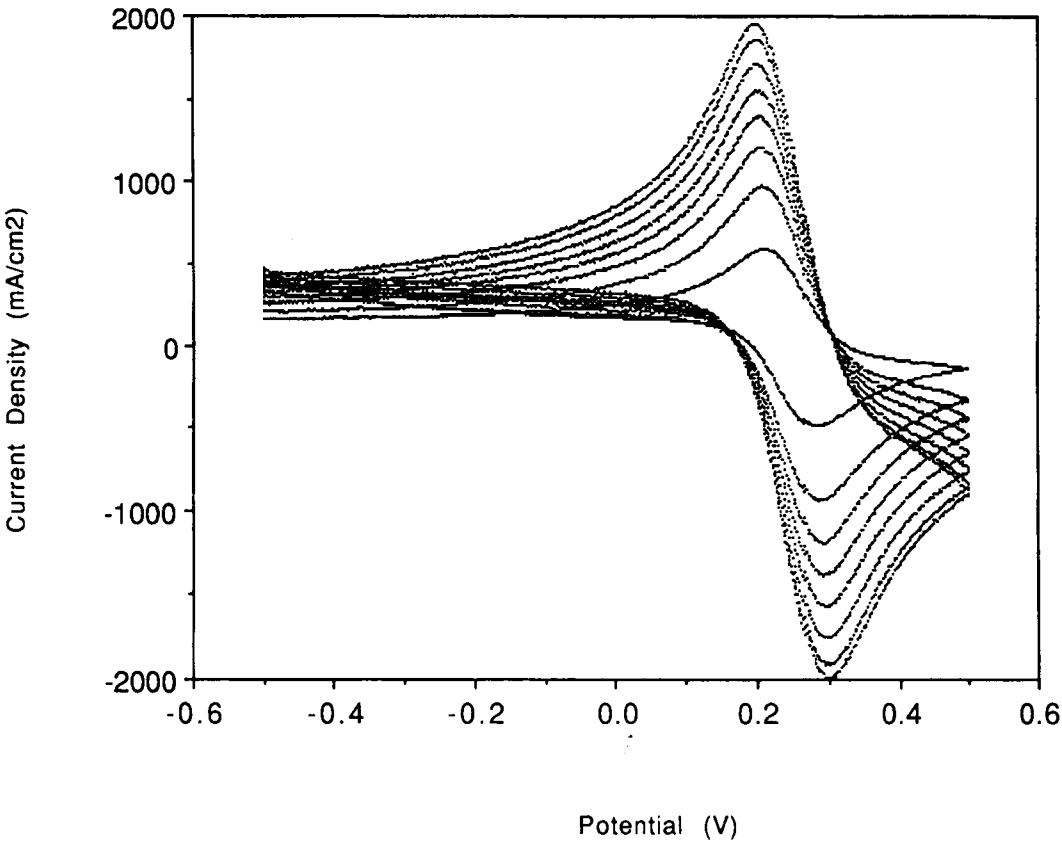

Fig. 24. Cyclic voltammetry results for 500 ppi phenolic-based porous carbon after methylene chloride cleansing.

is displayed by the 30 ppi phenolic-based porous carbon, which has the lowest SGSA.

For the fiber-based porous carbons, the higher the electrochemical area, the higher the SGSA (Table 7), in contrast to the phenolic-based porous carbons. This is because the mean pore sizes of all SUNY fiber-based porous carbons are smaller than those of all phenolic-based porous carbons (except 500 ppi), as shown in Table 3. As a result, the SUNY fiber-based porous carbons are not as penetrable by the electrolyte as all phenolic-based porous carbons except 500 ppi (Table 3). Thus, a large pore size is much more important than a large SGSA for attaining a large electrochemical area when the pore size is greater than about 100 μm, as in the case of phenolic-based porous carbons, though a large SGSA is more important than a large pore size when the pore size is less than about 100 μm, as in the case of fiber-based porous carbons.

Compared with glassy carbon (a solid carbon material, sample 22, Tables 4 and 5), the 400 μm fiber-based porous carbon with graphite flakes displays higher k_s, lower C and lower A, whereas the 500 ppi phenolic-based porous carbon (after methylene chloride cleansing) exhibits higher k_s, higher C and higher A. Carbon black and carbon paste (samples 23 and 21, respectively, Tables 4 and 5, both particulate carbon materials bound with oils) have much lower k_s than the 400 μm fiber-based porous carbon with graphite flakes or the methylene chloride cleansed 500 ppi phenolic-based porous carbon. On the other hand, carbon black has the highest C and A of all the carbons tested.

The mechanical, electrical and electrochemical properties determined for the porous carbons in this study allow the designer the ability to make judicious material selections for specific applications. For example, electrochemical applications requiring fast electron-transfer rate (high k_s), such as electrodes or catalysts, could be satisfied by 500 ppi phenolic-based porous carbon that was methylene chloride cleansed (if mechanical strength is unimportant) or a 400 μm fiber-based porous carbon with graphite flakes (if mechanical strength is important). For high electrochemical area and low capacitance, such as in catalyst supports, the plain fiber-based porous carbon fabricated with 50 μm long fibers could be used. On the other hand, for high electrochemical area and high capacitance in applications where rigidity is required, as might be the case for certain electrical devices, the 30 ppi phenolic-based porous carbon might be chosen. For other electrical applications requiring higher mechanical strengths and low electrical resistivities, the fiber-based porous carbons are preferred to the phenolic-based ones. If formability and particulate handling are required along with high capaci-

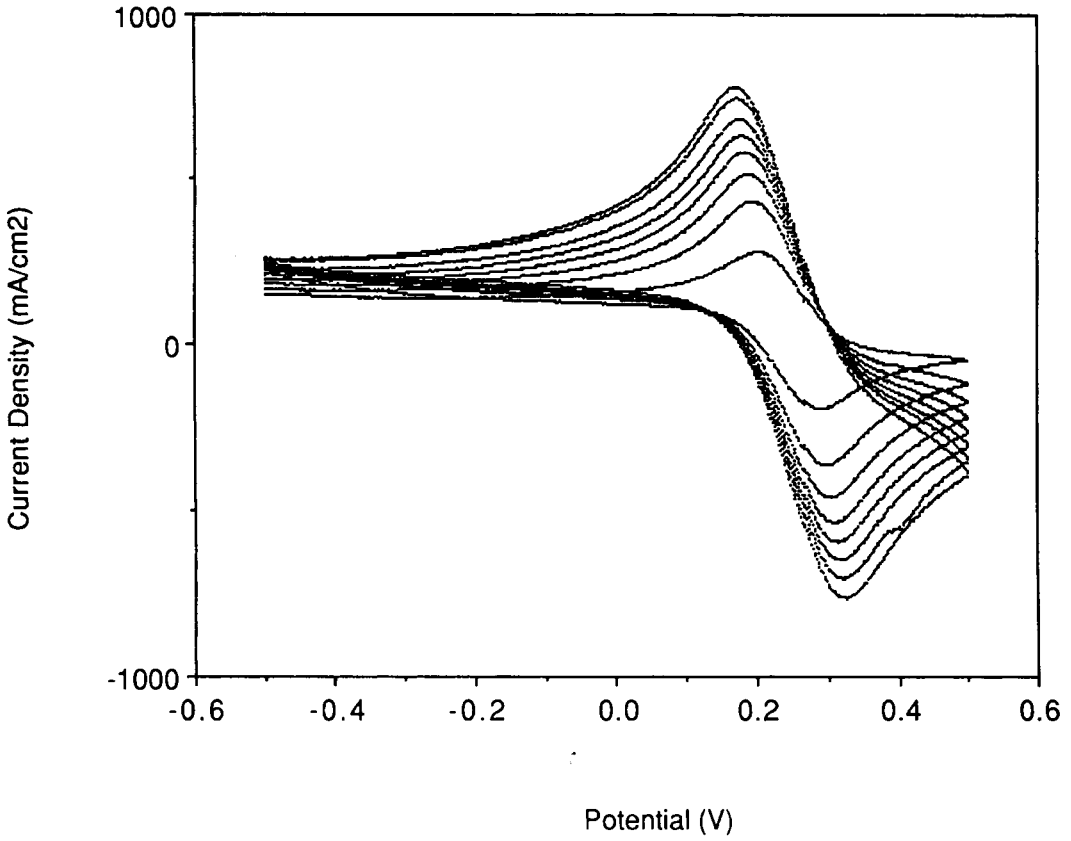

Fig. 25. Cyclic voltammetry results for 500 ppi phenolic-based porous carbon after TGA in nitrogen plus air.

tance, particulate carbon materials, specifically carbon black, would be the material of choice.

The mechanical and electrical properties of the fiber-based porous carbons studied in this work are, in general, superior to those of polymer-based porous carbons, because of their higher apparent density or lower porosity. (The fiber-based porous carbons increase in density as the fiber length decreases, due to the decreased porosity and pore size imparted by decreasing the fiber length.) Therefore, in spite of their inferior electrochemical behavior (in some cases), the fiber-based porous carbons may still be attractive for electrochemical applications that require good mechanical or electrical properties.

4. CONCLUSIONS

Porous carbons based on carbon fibers and those based on phenolic were evaluated electrochemically. Porous carbons based on carbon fibers exhibit irreversible electrochemical behavior unless graphite flakes or carbon black are added as coatings. The additives increase the electron-transfer rate constant k_s and capacitance C and decrease the electrochemical area A. Porous carbons based on phenolic exhibit much larger A than those based on carbon fibers, in spite of their lower geometric area. The electrochemical behavior of the porous carbon based on phenolic, however, varies from batch to batch due to contamination comprising $\leq 10\%$ of the porous carbon weight and primarily comprising long chain aliphatic hydrocarbons. This variation was removed by methylene chloride cleansing, which was found to improve the reversibility and increase k_s. Although heating removes the contamination by volatilization, the reversibility and k_s are less than those attained by methylene chloride cleansing. This suggests the importance of surface functional groups. Porous carbon based on phenolic (with 500 ppi and after methylene chloride cleansing) exhibit higher k_s, capacitance and electrochemical area than glassy carbon. Porous carbon based on carbon fibers (coated with graphite flakes), on the other hand, displays similar k_s, but lower capacitance and electrochemical area than glassy carbon. Among all the porous carbons tested, the highest electrochemical area and the lower geometric area are both attained by porous carbon based on phenolic with the lowest pore density (30 ppi); the high electrochemical area is due to the large pore size and the consequent good penetrability of the porous carbon by the electrolyte; the electrochemical area is even higher than that of carbon black. Among the porous carbons based on carbon fibers, the electrochemical area and the specific electrochemical area decrease with decreasing SGSA (increasing fiber length). Porous carbons based on

Table 7. Comparison of specific geometric surface area (SGSA) with electrochemical area and specific electrochemical area of porous carbons

Porous carbon[a]	Condition (cm^2/cm^3)	SGSA (cm^2)	Electrochemical area (cm^2/cm^3)	Specific electrochemical area
Based on carbon fibers				
1: P50	Plain	1030	58.1	4720
3: P100	Plain	968	29.7	1780
4: P400	Plain	455	23.9	1450
5: P400	Plus graphite flakes	735	9.3	1030
Based on phenolic				
8: 30 ppi	As-received	0.21	442.4	2590
9: 45 ppi	As-received	0.45	251.6	2620
10: 80 ppi	As-received	1.00	286.2	3030
14: 100 ppi	Methylene chloride cleansed	2.17	70.3	2410
18: 500 ppi	Methylene chloride cleansed	10.95	83.8	2870

[a]Sample numbers correspond to those of Table 4.

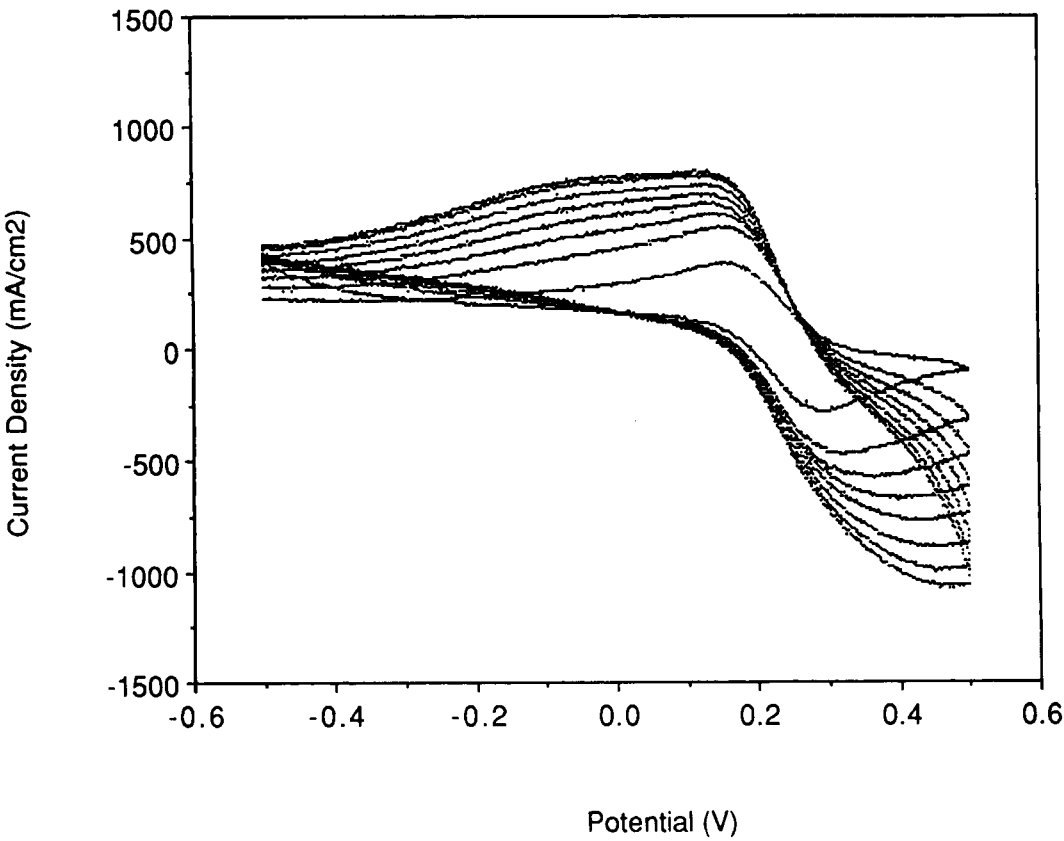

Fig. 26. Cyclic voltammetry results for 500 ppi phenolic-based porous carbon after TGA in nitrogen.

carbon fibers have higher apparent density, lower resistivity and higher compressive strength than those based on phenolic. Among porous carbons based on carbon fibers, the porosity, pore size and longitudinal/transverse electrical resistivity increase with increasing fiber length, whereas the compressive strength and geometric surface area decrease with increasing fiber length. The addition of graphite flakes to porous carbon based on carbon fibers increase k_s and decrease C and A, while increasing the compressive strength, slightly decreasing the porosity and slightly decreasing both longitudinal and transverse resistivity. Among porous carbons based on phenolic, the porosity, pore size, electrolyte penetrability and resistivity increase with decreasing pore density, while SGSA and compressive strength decrease with decreasing pore density.

Acknowledgements—The authors would like to thank the New York State energy Research and Development Authority for funding a part of this work.

REFERENCES

1. *U.S. Patent No. 3* 859 421 (1975).
2. Wang, J., *Electrochim. Acta*, 1981, **26,** 1721.
3. Strohl, A.N. and Curran, D.J., *Anal. Chem.*, 1979, **51,** 1050.
4. Blaedel, W.J. and Wang, J., *Anal. Chem.*, 1980, **52,** 76.
5. Agarwal, I.C., Rochon, A.M., Gasser, H.D. and Sparling, A.B., *Water Res.*, 1985, **18,** 227.
6. Sylwester, A.P., Aubert, J.H., Rand, P.B., Arnold, Jr. C., Clough, L.R., *Polym. Mater. Sci. Eng.*, 1987, **57,** 113.
7. Sylwester, A.P. and Clough, R.L., *Synth. Met.*, 1989, **29,** F253.
8. *U.S. Patent* 4 832 870 (1989).
9. Oren, Y. and Soffer, A., *Electrochim. Acta*, 1983, **28,** 1649.
10. Lestrade, C., Guyomar, P.Y. and Astruc, M., *Envioron. Technol. Lett.*, 1981, **2,** 409.
11. Guyomar, P. Y. Astruc, M. and Dubreuil J. P. *3rd Int. Conf. Heavy Met. Environ.*, 1981, p.80.
12. *Japanese Patent No.* J02053992-A 90.02.33 (9014) JP.
13. *Japanese Patent No.* J01266222-A 89.10.24 (8948) JP.
14. *Japanese Patent No.* J02106876-A 90.04.18 (9022) JP.
15. Hahn, C.S., Cho, H.S. and Yang, H.S., *Carbon*, 1981, **19,** 225.
16. Norwitz, G. and Galan, M., *Carbon*, 1967, **5,** 287.
17. Hagiwara, S., Tsutsumi, K. and Takahashi, H., *Carbon*, 1978, **16,** 89.
18. Matsumurta, Y., Hagiwara, S. and Takahashi, H., *Carbon*, 1976, **14,** 163.
19. Puri, B.R. and Bansal, R.C., *Carbon*, 1964, **1,** 457.
20. Kaye, G., *Carbon*, 1978, **2,** 413.
21. K. Kinoshita, *Carbon Electrochemical and Physicochemical properties*, Vol. 87, Wiley, New York, 1988, p. 297.
22. Frysz, C.A., Shu, X. and Chung, D.D.L., *Carbon*, 1994, **32,** 1499.
23. McCreery, R. L. *Electroanalytical Chemistry*, Ed. A. J. Bard, Marcel Dekker, New York, 1989, p. 306.
24. Strein, T.G. and Ewing, A.G., *Anal. Chem.*, 1991, **63,** 194.
25. Wightman, R.M., Deakin, M.R., Kovach, P.M., Kuhr, W.G. and Stutts, K.J., *J. Electrochem. Soc.*, 1984, **131,** 1578.
26. *Fiberform Product Literature*, Fiber Materials Inc. Biddeford, ME, 1987.
27. *Reticulated Vitreous Carbon Product Brochure*, The Electrosynthesis Co. Inc., 1976.
28. Runyan, W. R. *Semiconductor Measurements and Instrumentation*, McGraw-Hill New York 1976, p. 69.
29. Shui, X., Frysz, C.A. and Chung, D.D.L., *Carbon*, 1995, **33,** 1681.